PCCP

Physical Chemistry Chemical Physics

www.rsc.org/pccp

Volume 15 | Number 12 | 28 March 2013 | Pages 4075–4460

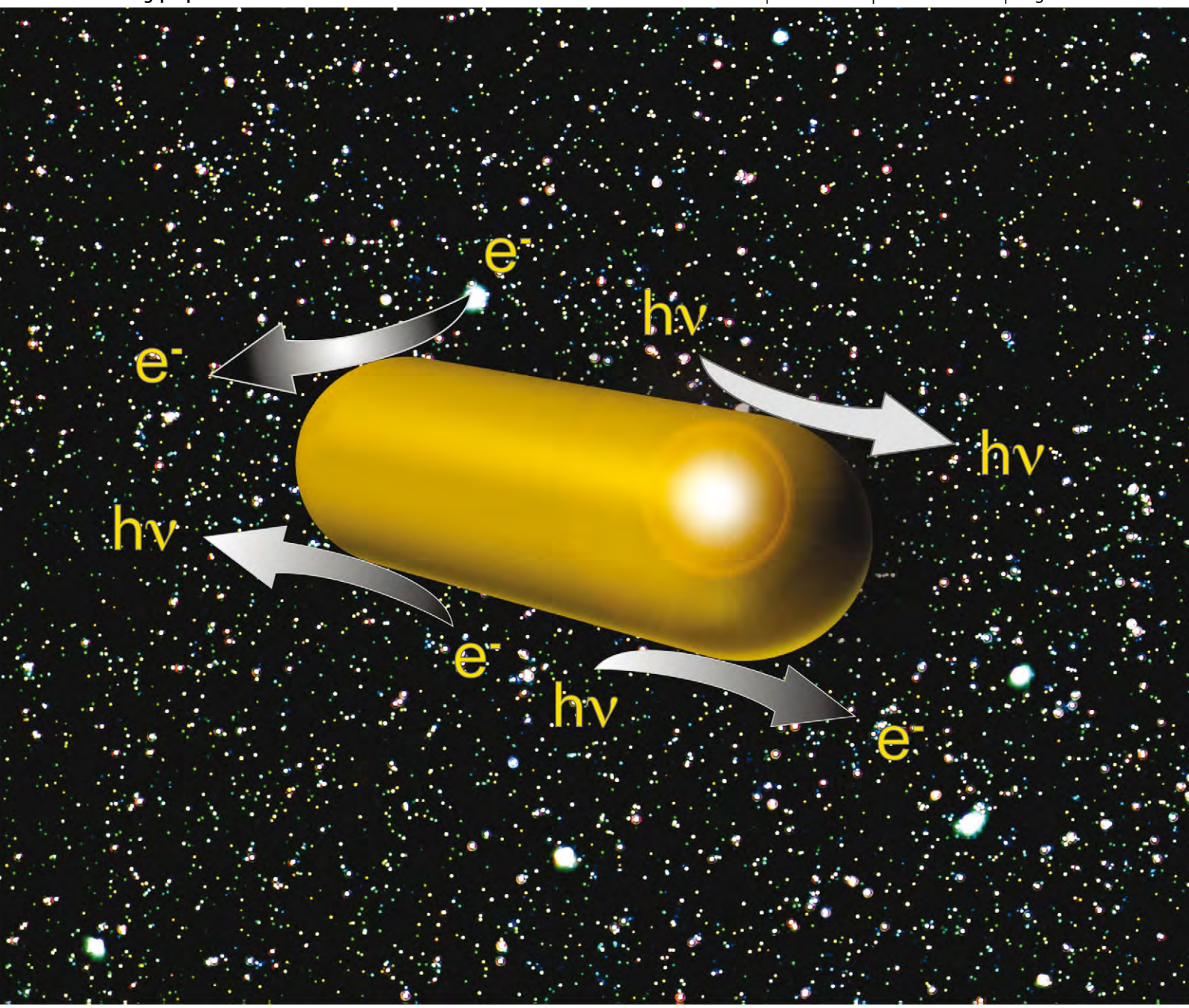

ISSN 1463-9076

PERSPECTIVE
Ringe *et al*.
Single nanoparticle plasmonics

1463-9076(2013)15:12;1-T

PCCP

RSC Publishing

PERSPECTIVE

View Article Online
View Journal | View Issue

Single nanoparticle plasmonics

Cite this: *Phys. Chem. Chem. Phys.*, 2013, **15**, 4110

Emilie Ringe,†*[a] Bhavya Sharma,[a] Anne-Isabelle Henry,[a] Laurence D. Marks[b] and Richard P. Van Duyne[a]

Received 18th December 2012,
Accepted 4th February 2013

DOI: 10.1039/c3cp44574g

www.rsc.org/pccp

Interest in nanotechnology is driven by the unique and novel properties of nanoscale materials such as the strong interaction of metal particles with light, caused by localized surface plasmon resonances (LSPRs). In this perspective article we review and discuss prominent advantages and advances in single particle studies of plasmonic nanostructures. Common techniques and recent improvements in spatial and spectral resolution will first be outlined, covering both far-field and near-field phenomena. Then, new insight and information uniquely obtained from single particle approaches will be overviewed, including several fundamental studies of plasmonic behaviour, as well as applications using single particle tracking and chemical reaction monitoring. Finally, highly interdisciplinary future directions and experiments are discussed.

1. Introduction

The optical properties of nanoparticles have been observed since the antiquity, for example, as part of the 4th century AD Lycurgus cup and medieval stained glass. Scientific interests in the colour of small particles debuted later, when Faraday synthesized the famous ''Ruby Fluid'' by reacting gold chloride with phosphorous in ether.[1] Faraday recognized that the colour was due to the reduction of gold to small particles, and later Mie provided the theoretical foundations explaining the colour of the particles and its dependence on metal composition as well as surrounding environment.[2]

Such bright colours arise in materials with a negative real and a small positive imaginary dielectric constant in a given

[a] *Department of Chemistry, Northwestern University, Evanston, IL 60208, USA. E-mail: er407@cam.ac.uk*
[b] *Department of Materials Science and Engineering, Northwestern University, Evanston, IL 60208, USA*
† Current address: Department of Materials Science and Metallurgy, University of Cambridge, Cambridge CB2 3QZ, UK.

Emilie Ringe

Emilie Ringe is a Gott Junior Research Fellow at Trinity Hall, Cambridge University, as well as a Newton International Research Fellow (the Royal Society, UK). She studied at McGill University at the undergraduate level before obtaining a MS from Northwestern University in inorganic crystallography with J. A. Ibers. She then completed a PhD in optical spectroscopy and analytical modelling of nanoparticle shape in the groups of Richard Van Duyne and Laurence Marks at Northwestern University in 2012. She currently works in the high resolution electron microscopy group at Cambridge University; her research interests include atomic resolution elemental mapping of alloy nanoparticles relevant for catalysis applications, as well as near-field plasmon mapping using electron energy loss spectroscopy.

Bhavya Sharma

Bhavya Sharma received her BS in Exercise Science at SUNY Buffalo. She completed her PhD in 2011 in Chemistry from the University of Pittsburgh under the guidance of Prof. Sanford Asher. She used UV resonance Raman spectroscopy and excitation profiles to examine electronic transitions in peptides and proteins. Bhavya is currently a postdoctoral fellow with Prof. Richard P. Van Duyne at Northwestern University. Her research interests include biological applications of SERS and Raman spectroscopy and Raman imaging.

wavelength range, such as quasi-free electron metals, Ag, Au, Cu, and Al, because they can support surface plasmon resonances (SPRs) when submitted to electromagnetic radiation. The SPR can be of two types: propagating or localized. Propagating surface plasmons, also called surface plasmon polaritons (SPP), are oscillations of electric charges travelling at a metal–dielectric interface. In small metallic particles such as Faraday's "Ruby Fluid", the electron oscillation becomes localized, and is thus called localized surface plasmon resonance or LSPR. This particle-confined oscillation occurs in the entire particle, however the strongest electric fields are found at the metal–dielectric interface (hence the name "surface"). Three wavelength-dependent phenomena arise from LSPR: enhancement of the electric field on the surface of the particle, photon absorption, and photon scattering. The latter two are directly responsible for colour, while the former gives rise to the electromagnetic contribution in surface-enhanced spectroscopies.

Anne-Isabelle Henry

Anne-Isabelle Henry received a BS in physical chemistry from University Paris Sud (2003) in Orsay, France after completing an internship in the Department of Physical Chemistry at the Fritz Haber institute in Berlin, Germany. She received a PhD (2008) in chemistry from University Pierre and Marie Curie in Paris, France on the thermal stability and control of superstructure in Ag nanocrystals assemblies. She is currently a senior research associate at Northwestern University. Her research interests include the fabrication, assembly, and study of plasmonic nanoparticles, SERS-active nanoparticle aggregates and substrates with a focus on structure–property relationships.

Several factors affect the LSPR behaviour of nanoparticles, including shape, size, composition, dielectric environment, providing exquisite tuneability as well as characterization challenges. Given the complex and acute dependence of plasmonic properties on structural factors, even optimized synthesis products contain shape inhomogeneities which prevent obtaining quantitative information from bulk measurements. Just as biological processes can be better understood from single biomolecule studies,[3] and nanoparticle dynamics such as vibration are best unravelled one particle at a time,[4] knowledge on plasmonic behaviour can be uniquely enhanced by single particle approaches. Technical and instrumental advances have greatly increased their robustness, reliability, and popularity, producing an increasingly vast body of literature on plasmonics studied at the single particle level.

In this perspective, we will highlight the most prominent tools and unique features of single particle spectroscopy, focusing on the characterization of plasmonic phenomena in colloidal nanoparticles. In Section 2, the most common tools as well as recent advances in characterization of single nanoparticles will be reviewed. Then, in Section 3, examples of recent findings will be discussed with a focus on what can uniquely be learnt from single particle approaches. Finally, Section 4 concludes with open challenges and future directions. Note that since all the particles discussed herein are nanosized, we decided to omit the 'nano' prefix for simplicity, *i.e.*, a nanosized rod will be referred to as a rod rather than a nanorod; for analogous reasons we will refer to quasi-spherical particles as sphere, although true spheres are very rare because of faceting and twinning tendencies.

2. Methods and advances in single particle characterization

A surface plasmon is by definition a polariton, *i.e.* a photon coupled to an electron,[5,6] such that either photons or electrons

Laurence D. Marks

Laurence D. Marks received his BA in chemistry and a PhD in physics from Cambridge University. Marks did postdoctoral training in Cambridge with Drs D. J. Smith and A. Howie as well as with Prof. J. M. Cowley at Arizona State University. Since 1985 he has been a faculty member at Northwestern University. He has research interests in a range of areas, from nanoparticles to nanotribology and surface science.

Richard P. Van Duyne

Richard P. Van Duyne is Charles E. and Emma H. Morrison Professor of Chemistry and of Biomedical Engineering at Northwestern University. He received a BS (1967) at the Rensselaer Polytechnic Institute and PhD (1971) at the University of North Carolina, Chapel Hill, both in chemistry. He is a member of the National Academy of Sciences and the American Academy of Arts and Sciences. He is known for the discovery of surface-enhanced Raman spectroscopy (SERS), the invention of nanosphere lithography (NSL), and development of ultrasensitive nanosensors based on localized surface plasmon resonance (LSPR) spectroscopy.

can be used to excite this fascinating electron oscillation. A large number of experimental approaches are thus available to excite and probe the plasmonic behaviour of single particles, offering a rich variety of information and resolution. In this section, we describe the most commonly used single particle characterization methods, as well as recent and exciting advances, and explain what unique information they are capable of providing. For quick reference, the main characteristics of each technique are presented in Table 1.

2.1 Far-field approaches to single particle characterization

While nanoparticles cannot be directly observed with the naked eye, the effects of their plasmonic behaviour can readily be visualized in, for example, the bright colours in medieval stained glass. Methods probing the optical properties of nanoparticles from a distance much larger than the wavelength of light, *i.e.* far-field approaches, are simple and robust tools to study some of the prominent features of plasmonic particles. Despite being intrinsically diffraction-limited, far-field approaches are useful to analyse absorption and scattering properties, while the plasmon-induced electric field can indirectly be characterized through enhancement factors in various types of spectroscopies. Additionally, far-field detection simplicity allows for its incorporation in more complex experimental schemes such as dynamic tracking and correlation with structural parameters, enabling the study of complex, heterogeneous systems.

2.1.1 Scattering by plasmonic nanoparticles. Light scattering is a common phenomenon that occurs whenever a refractive index contrast exists between a particle and its surroundings. In plasmonic particles, elastic photon scattering is strongly wavelength dependent and is most enhanced at the resonance frequency. Single particle light scattering was first observed about a century ago by Zsigmondy, whose ultramicroscope and studies of colloids were rewarded by the 1925 Nobel Prize in Chemistry.[19] Dark-field optical microscopy (herein referred to as simply dark-field microscopy) is now a prominent nanotechnology tool.[20–30]

Table 1 Overview of single particle detection techniques

	Technique	Probed phenomenon	Spatial resolution	Advantages	Disadvantages
Far field	Dark-field microscopy	Scattering	Diffraction limited	Simple platform easily coupled to other techniques Dynamic nanoparticle tracking Single molecule detection[7]	Background scattering from other objects Typically limited to large particles (>40 nm)[8,9]
	Photothermal imaging (PHI)	Absorption	Diffraction limited	Low background interference Single molecule detection[10] Detection of very small particles (1.4 nm)[11]	No direct cross-section information Needs relatively intense pump sources
	Spatial modulation spectroscopy (SMS)	Extinction	Diffraction limited	Provides absolute extinction cross-section No intense pump sources required	Less sensitive than PHI Requires larger particles (>5 nm)[12]
	Surface-enhanced spectroscopy	Electromagnetic field enhancement	Diffraction limited	Direct probing of performance for spectroscopic applications	Indirect characterization of the near-field Enhancement factor provides an averaged field intensity
Near field	Scanning near field optical microscopy (SNOM)	Near-field optical transmission or scattering	<10 nm (aperture-less probe)[13]	Wide spectral range and good energy resolution Flexible measurement capabilities and geometries Suitable for non-vacuum and liquid environment	Possible near-field perturbation from the probe
	Photoelectron emission microscopy (PEEM)	Photon-induced, field-enhanced electron emission	20–25 nm[14] 2 nm (aberration-corrected)[15]	Can be coupled to other techniques (2-photon photoemission, interferometric pump–probe techniques) Good spatial resolution	Requires sophisticated electron optics Possible distortions due to charging
	Scanning photoionization microscopy (SPIM)	Photon-induced, field-enhanced electron emission	Diffraction limited	High temporal resolution Relative simplicity Polarization studies possible	Indirect near field information Limited energy resolution
	Cathodoluminescence	Electron-induced, field-enhanced photon emission	10–50 nm[16,17]	Can be performed in TEM or SEM Relatively simple instrumentation	Sample must be stable under electron beam Spatial resolution intrinsically limited by electron–hole recombination distance
	Electron energy loss spectroscopy	Energy loss in transmitted electron beam due to plasmon excitation	Sub-Å[18]	Best spatial resolution achievable Fitting of STEM-EELS data can yield deconvoluted modes Simultaneous elemental analysis possible	Sophisticated, expensive equipment required Possible difficulty in analysis to due to plasmon modes overlap Requires stable and electron transparent sample

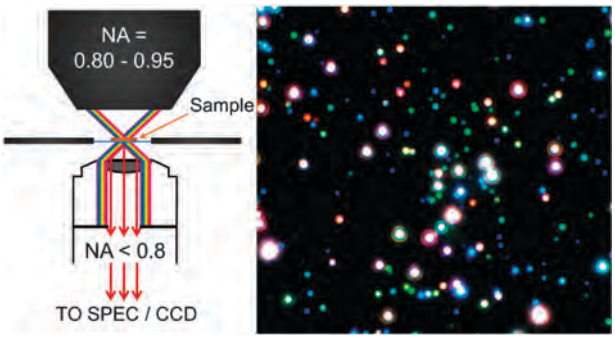

Fig. 1 Dark-field microscopy. Left: schematic of the experimental geometry showing the hollow cone of white light illuminating the sample. Right: real-colour image of the scattering from colloidal nanoparticles on glass. Left and right panels reproduced with permission from ref. 149 and 23, respectively.

In summary, a high numerical aperture dark-field condenser, where the central portion of the cone of light is blocked, is used to illuminate the sample with a hollow cone of light as depicted in Fig. 1. The smaller numerical aperture collection objective accepts only light scattered by particles in the field of view, giving rise to a dark background (hence "dark-field") with particles of various shapes and sizes appearing as bright spots of different colours and intensities against a black background (Fig. 1).

The variation of scattering intensity can be in part attributed to size effects, as explained by Mie theory,[2,31] a simple and well-known way to model the extinction (scattering + absorption) of a plasmonic particle.[29] While this solution to Maxwell's equations describes the peak position (colour) dependence on volume for spheres,[32] other approaches (numerical or experimental) are needed for non-spherical particles. Scattering studies can, in general, probe single particles as small as 35 nm,[22,23] depending on their composition. To lower this size limit, various approaches have been combined with dark-field microscopy, such as polarization effects,[26,27,33,34] supercontinuum white light sources,[21] and spatial modulation spectroscopy.[35,36] These new developments have allowed for particles as small as 5 nm in size to be imaged.[21]

2.1.2 Absorption by plasmonic nanoparticles. Despite the advances in detection limits mentioned above, the observation of nanoparticles *via* scattering methods becomes increasingly difficult as their size decreases. Indeed, as described in Mie theory[2] (and more generally in Rayleigh's theory[37]) the scattering cross-section of a nanoparticle much smaller than the wavelength of light scales as the sixth power of its radius, while the absorption cross-section scales as its third power. It becomes immediately evident that absorption-based methods are better suited than scattering-based ones for the detection of nanoparticles with radii smaller than 50 nm.[29,38] Furthermore, detection of low intensity scattering can be impeded by a variety of background signals from non-plasmonic impurities in the sample, complicating data acquisition and processing.

While several methods have been reported for measuring the absorption of photons by single metal nanoparticles,[8,31,38–41] the two most commonly used are photothermal imaging and spatial modulation spectroscopy. The former was pioneered by Boyer *et al.*[8] and later refined by Berciaud *et al.*[11,39] as photothermal heterodyne imaging (PHI); an alternative and more explicit name, LISNA (Laser induced scattering around a nanoabsorber), is also present in the literature.[40] This method takes advantage of the slight refractive index change resulting from heat release around an excited object; any absorbers, including plasmonic nanoparticles, can be detected at room temperature without background interference. PHI has been used to measure the absorption of supported Au particles as small as 5 nm in diameter[42] and ~1.4 nm (67 atom clusters),[11] as well as 5 nm Ag nanoparticles.[39] Beyond fundamental studies of single nanoparticles immobilized on a substrate, PHI is also a powerful, low background approach to detect freely diffusing nanoparticles in complex media, as will be discussed in Section 3.[43] The signal-to-noise ratio of photothermal microscopy[44] can typically be improved by increasing the power of the laser beam probe, increasing the magnitude of the temperature-dependent refractive index change of the surrounding medium (organic solvents, thermotropic liquid crystals[45]), and thermally isolating the absorber from the glass substrate.

Spatial modulation spectroscopy (SMS) is another technique to characterize very small particles by monitoring the extinction of a light beam (laser, white light, or supercontinuum) caused by the passage of a single nanoparticle, providing a single particle extinction spectrum (*i.e.* absorption and scattering combined). Fig. 2 provides a graphical description of this principle, and further experimental details can be found in a recent review.[12] Beyond measuring the absolute extinction cross-section of single nanoparticles,[12] SMS can characterize changes in refractive index around particles *via* extinction changes.[46]

These two absorption-based techniques, PHI and SMS, can be correlated with other types of spectroscopy or imaging, providing a powerful platform for the investigation of plasmonic properties. The simultaneous acquisition of absorption (*via* PHI) and fluorescence data[47] shows promise for applications in multidimensional tracking and sensing, while correlation with electron microscopy allows the study of fundamental size and shape effects.[29] Such recent developments and growth of novel far-field optical techniques provide new ways to study single particle absorption, hereby expanding the set of measurables available to researchers for fundamental plasmonic investigation as well as applications in biological and other complex media.

2.1.3 Surface-enhanced effects. Plasmon resonances in small metal particles induce strong electric fields at the particle/dielectric interface, typically orders of magnitude more intense than the incoming radiation. This enhancement can be utilized to increase the signal of optical spectroscopies such as Raman and fluorescence. Surface-enhanced Raman spectroscopy (SERS) is a powerful vibrational technique that allows for highly sensitive and selective detection of low concentration analytes through this plasmonic amplification of electromagnetic fields. The electromagnetic enhancement mechanism is generally believed to be the primary contributor to the SERS effect, while the chemical mechanism, which primarily results from charge transfer between the metal and molecule, provides a minor enhancement effect.

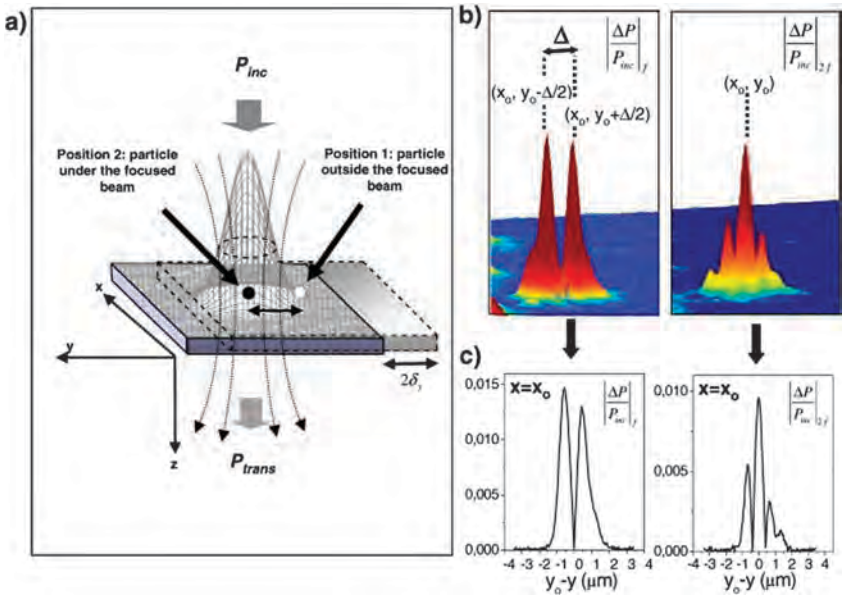

Fig. 2 Spatial modulation spectroscopy. (a) Experimental geometry showing incoming light focused close to the diffraction limit on the sample plane. (b) Spatially resolved transmission intensity change for a Au nanoparticle at λ = 530 nm, with lock-in amplifier set at the position modulation frequency (f) and its first harmonic (2f). (c) Cross-section of the transmission change. Reproduced with permission from ref. 12.

In the electromagnetic enhancement mechanism, the regions of high electromagnetic fields, known from near-field measurement and calculations to be located in gaps, crevices, and at sharp features of nanoparticles, generate sites of high signal enhancement, commonly referred to as "hot spots" (Fig. 3). The hot spot phenomenon is a complex subject reviewed elsewhere.[48,49] Typically, the enhancement due to both mechanisms is reported as an enhancement factor (EF), which is calculated as a ratio between the SERS intensity and the normal Raman intensity of an analyte:[49,50]

$$EF = (I_{SERS}/N_{SERS})/(I_{NRS}/N_{NRS})$$

where I_{SERS} and I_{NRS} are the SERS and normal Raman scattering intensities, respectively, and N_{SERS} and N_{NRS} are the number of molecules contributing to the scattering intensity, typically calculated as surface coverage in SERS and as a scattering volume in the solution for the normal Raman. In general, the electromagnetic enhancement mechanism contributes EFs up to $\sim 10^8$–10^9, while the chemical mechanism contributes EFs $\sim 10^2$–10^3.[50–54] Resonance Raman effects can further produce an enhancement on the order of 10^3–10^4.[55,56] When multiplied ($EF_{total} = EF_{SERS} \times EF_{ResRaman}$), these enhancements can yield the theoretically possible total EFs of 10^{14}–10^{16}.[49,54,56–58] This combination of SERS with the resonance Raman effect gave rise to the EFs $\sim 10^{14}$–10^{15} reported in the first single molecule SERS papers.[57,59,60] Careful examination of experimental SERS EFs can generate information about the "average" electric field enhancement around a particle or cluster of particle, leading to better understanding of plasmonic phenomena. In addition to this plasmonic characterization application, its small probing volume and high signal enhancement make SERS powerful in very low concentration sensing.

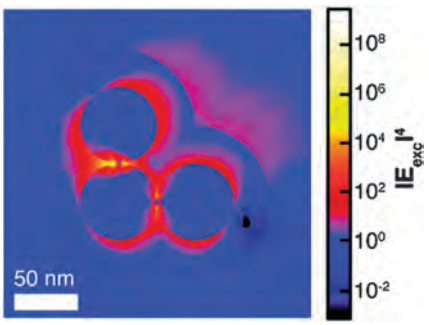

Fig. 3 Finite element method calculation results for a L-shaped trimer SERS nanoantenna. The antenna-averaged electromagnetic enhancement ($|E_{exc}|^4$) is plotted as a heat map demonstrating two hot spots located at the junction between two spheres. Reproduced with permission from ref. 156.

Second harmonic generation (SHG) spectroscopy is another far-field, surface-enhanced spectroscopy that can be used to probe the plasmon-induced electric field enhancement. SHG is a non-linear optical process where photons interact with a non-linear material through which two photons are combined to produce one photon with double the frequency (half the wavelength). An attractive surface and interface probing technique, SHG has unique advantages such as detection of sub-monolayer coverage and sub-ps time resolution.[61] Furthermore, high-resolution imaging depths of hundreds of microns are achievable by using wavelengths in the near-IR range.[62] SHG has been most successfully used with imaging microscopy, which allows for high resolution and rapid data acquisition, especially when combined with laser scanning technology; direct visualization of sample structure, with no need for exogenous dyes or contrast agents, can be achieved. Also, because signals arise from induced polarization instead of, as

in the case of fluorescence, from absorption, photobleaching and phototoxicity are reduced. Beyond imaging, intrinsic nonlinear optical properties of nanoparticles such as hyperpolarizability and polarization-dependent behaviour can be measured *via* SHG.[63,64]

2.1.4 Dynamic particle tracking. Tracking the plasmonic response of a particle over a long period of time provides information about real-time diffusion coefficients,[22] adsorbate-induced changes in the plasmon resonance maximum (LSPR λ_{max}),[23] and effects of varying nanoparticle dimensions.[25] Far-field imaging techniques, in particular scattering, are ideally suited to dynamic tracking of nanoparticles because no direct contact with the sample is required, and the addition of nanoparticles is believed to minimally interfere with biological processes.[65] Noble metal nanoparticles are easily trackable probes for different systems because of their large scattering cross sections at LSPR λ_{max}, rendering them extremely bright. While the spatial resolution for discerning two identical nanoparticles is generally diffraction limited ($\sim$250 nm),[66] several strategies have been developed to improve the spatial resolution of far-field techniques, which can now reach 1–10 nm. Such approaches include binding of nanoparticles with fluorescence markers (generally referred to as fluorescence nanoscopy[67]), combination of high speed video microscopy with fluorescence,[68] photothermal imaging,[40] use of improved instrumentation such as liquid crystal[22] or acousto-optic tuneable filters in conjunction with electron-multiplying CCD cameras,[69] combining dark-field microscopy with polarization,[70] and employing more intense white light (femtosecond white light continuum) sources.[71] Under optimal conditions, some of these advanced techniques even allow the detection of particles a few nanometres in size, although for biological systems, particles larger than 30 nm are more clearly visible amongst the complex environment.[65]

2.1.5 Correlation with structural characterization. The fine relationships linking plasmonic response to the size, shape, and composition of metal nanoparticles allows for exquisite control over their optical properties. Quantifying this dependence and unravelling its details is thus critical to both fundamental understanding and application development. Inevitable structural inhomogeneities in colloidal synthesis products, however, are major obstacles to the use of bulk solutions as only general trends can be extracted from such ensemble-averaged measurements, rather than the quantitative relationships gained from single particle studies. Single particle far-field approaches are well suited to optically characterize a large number of individual particles as the data acquisition is typically fast and correlation with high resolution structural measurements can provide the high quality information and large data sets necessary to extract quantitative relationships.

While simultaneous far-field optical response and structure can be obtained, for example with total internal reflection spectroscopy coupled with atomic force microscopy,[72] the use of *ex situ* structural characterization dominates because of the superior structural resolution achieved by electron microscopy. Scanning and transmission electron microscopes (SEM and TEM) offer different advantages and limitations and are typically chosen according to the sample studied. Structural characterization with SEM is completely substrate-general, although the best imaging resolution can be achieved on a conductive support film. Because of its transparency (allowing transmission geometries for optical characterization) and its conductivity, indium tin oxide (ITO) is ideally suited for correlative work and is broadly used despite some minor background (both in scattering and imaging) due to surface roughness. When using a TEM, likely chosen because of its unmatched structural resolution or analytical capabilities, electron transparent substrates are required. A variety of film composition can be purchased or fabricated, including formvar (polyvinylformal), amorphous carbon, graphene, SiO_x, Si_3N_4, and Si; optical transparency is of course not an issue, but small grid spacing or deep etch pits can cause problems by scattering strongly or blocking low angle incoming light. Substrate effects, due to the inhomogeneous environment around the particle[73–76] can be eliminated, if desired, by immersing the sample in a solvent with a matching refractive index.[77]

Particle retrieval techniques for correlated measurements are essentially the same regardless of substrate. In most cases, a group of particles of interest or region of interest is typically associated with an easily retrievable marker, either random or fabricated. In the random case, large aggregates and particle location patterns[78] provide guidance, sometimes in conjunction with grid bars or asymmetric patterns built in the substrates.[73,74,79–81] Examples of deliberate markers used include ITO etch pits milled with an ion-beam,[24] lithographically fabricated metal patches,[63] and alignment marks created by evaporation.[30] Such markers allow easy retrieval of the particles for structural characterization after the optical experiments are performed. Because of the low damage inflicted upon imaging at low magnification in a SEM, rough structural characterization can be performed first (identifying aggregation state for example), without major effects on the optical properties.[82] Damage, evidenced by plasmon frequency shifts and broadening, is however observed for most Ag nanoparticles as well as for prolonged imaging, such that control experiments are necessary for each new system. Note that due to damage and potential contamination yielding large redshifts of the LSPR resonance,[83] it is impossible to image with a TEM before optical characterization.

Far-field optical methods such as scattering and absorption can thus provide information with high energy resolution, capable, when coupled to electron microscopy, of unravelling fine details of the size and shape-dependence of plasmon energy, polarization, refractive index sensitivity, and plasmon decay. Additionally, SERS and other surface-enhanced spectroscopies allow the quantification of the field enhancement around the nanoparticle(s).

2.2 Near-field approaches to single particle characterization

While the far-field techniques discussed above provide access to much-needed quantitative understanding of structural effects, their intrinsic diffraction-limited resolution impedes access to detailed information about the underlying electron oscillation phenomenon. A detailed knowledge of the position-dependent oscillation amplitude (which does not necessarily

peak at the same energy as the far-field observations as explained in ref. 84) within and around the particle can unravel regions of high field enhancement critical to sensing performance optimization. This understanding can be gained using various forms of electric field mapping which allow the direct visualization of the plasmon eigenmodes. Additionally, dipole forbidden modes, which cannot be excited by far-field approaches, are accessible *via* local excitation.[85,86] Many techniques exist, combining or relying solely on photons and/or electrons. Some of these have been reviewed recently,[5,13,17,87] such that this section will only briefly overview the standard techniques and most exciting developments.

2.2.1 Near-field optical microscopy. Near-field optical techniques aim at improving the spatial resolution limits of far-field optical techniques while preserving their excellent energy resolution by introducing a physical, optical probe in close proximity to the particle,[5,13,87–93] a concept first outlined by Synge in 1928.[94] Akin to topographical mapping, the spatial resolution of near-field optical techniques is largely determined by the nature and sharpness of the probe.

In scanning near-field optical microscopy (SNOM), a tip is scanned a few nanometres above the sample deposited on an optically transparent substrate, creating localized illumination, and the transmitted or emitted light is collected by either a high numerical aperture objective (positioned above or below the sample) or the tip itself.[13] Reflective geometries have been developed such that a variety of substrates can also be accommodated.[90] An important drawback of this technique is the possible (and difficult to assess) distortion of near-fields caused by the presence of the probe, such that care must be taken to balance spatial resolution (closer probes give better resolution) and near-field disruption (minimized by distant probes).

Traditional SNOM probes fabricated by chemical etching and metal coating of a fibre followed by aperture fabrication yield emission aperture dimensions of the order of tens of nanometres. This most common experimental geometry is referred to as aperture-type SNOM, and its resolution is typically of the order of several tens of nanometres (50–100 nm).[95] Recent advances in tip fabrication and design have improved the spatial resolution of SNOM: a prominent development being that of apertureless, or scattering-type SNOM[13,87,96] which can reach less than 10 nm spatial resolution by using needle-like probes; as in scanning tunnelling microscopy resolution is determined by the radius of curvature of the probe. Improvement in resolution have been predicted and observed using patterned tips acting as waveguides.[97–99]

The flexibility of the light input and experimental geometry in SNOM allows for a large number of optical experiments, many of which have been proposed or realized. Non-linear phenomenon providing information on plasmon dynamics, such as two-photon luminescence,[91,100,101] have been successfully coupled to SNOM. Ultrafast experiments are also possible.[87] Overall, while the perturbation potential and limited spatial resolution of SNOM place it as a disadvantage compared to other near-field techniques, its wide spectral range, excellent energy resolution and flexible measurement capabilities ensure its lasting presence in the plasmonics field.

2.2.2 Photoemission. The interaction of photons with metallic materials leads to electron emission when an energy beyond the workfunction can be reached, a phenomenon utilized in ultraviolet and X-ray photoelectron spectroscopy (UPS and XPS).[102] When plasmonic metals are probed, however, a significant increase in electron emission can occur due to the local electric field enhancement produced by plasmon resonances, such that information on the near-field patterns can be obtained from the position-dependence of electron emission intensity. This capability is harnessed in a common and commercially available approach called photoelectron emission microscopy (PEEM), which has been used to map, with a resolution down to 20 nm, the photoemission enhancement in a number of patterned surfaces,[103–105] slits,[106] and a small number of single particles including crescents.[107]

Recent advances have coupled PEEM with 2-photon photoemission as well as sophisticated interferometric pump–probe approaches yielding improved contrast;[104,108] coupling with femtosecond excitation has also been achieved to probe ultrafast processes,[105,106,109–111] while aberration correction improved the lateral resolution down to a few nanometres.[15,112] PEEM, however, can be a complex tool requiring sophisticated electron optics and special care to avoid distortions due to charging. A diffraction-limited variant of the technique, scanning photoionization microscopy (SPIM), has been developed and used to study the behaviour of plasmonic particles such as rods and cubes;[80,113–115] its high temporal resolution and relative simplicity are prominent advantages.

2.2.3 Cathodoluminescence. Electrons can be used as a broadband point dipole source to excite plasmon resonances, such that one can detect and locally map plasmonic behaviour by monitoring the events accompanying electron excitation. Photons are emitted by the probed material as a result of this excitation, a process called cathodoluminescence (CL). In CL spectroscopy, high spatial resolution is obtained by controlling at the nanometre level the position of the excitation beam; the detection consists of measuring the number and the energy of photons emitted, usually through a large area detector or parabolic mirror.[16,116] CL can be performed in both TEM and SEM, the latter being more common because of lower costs, easier implementation, and the ability to use thick or low background substrates such as Si wafers.[16] Spectrally resolved CL yields either a spectra at each beam position or an image for a selected energy, while panchromatic CL (panCL) provides intensity-only information by collecting all the light emitted regardless of energy. The lateral resolution of the obtained images is typically quite large, however, as it is not only limited by the size of the electron beam, but also by the potential emission near (not only at) the electron beam position, a fundamental property of the CL process.[16] Current best lateral and spectral resolutions are of the order of a few (5–10 nm) and a few tens (20–50) of nanometres, respectively.[16,17] Scanning tunnelling luminescence, a modification of scanning tunnelling microscopy, shows promise toward improving the spatial resolution. However, the required short tip–sample distance can be a problem for observing particles of plasmonically relevant sizes and shapes.[117]

2.2.4 Electron energy loss microscopy. Electrons can transfer energy to a nearby metallic particle to excite a plasmonic resonance, such that detecting the change in energy, *i.e.* energy loss, of transmitted electrons provides a high spatial resolution approach to obtain a scattering probability map in and around a single metallic nanoparticle. As in CL spectroscopy, two techniques can be utilized to unravel information about the electron oscillation behaviour of a nanoparticle: scanning transmission electron microscopy electron energy loss spectroscopy (STEM-EELS)[85,118,119] or energy-filtered transmission electron microscopy (EF-TEM).[120] In the former, a small electron beam (~1 nm in diameter) is scanned across the sample, and a full energy-loss spectrum is acquired at each point. Field distributions for each peak can then be reconstructed from peak fitting. In the latter, a full image is acquired at a small specific electron energy window, and a spectrum can be obtained by extracting the intensity of a pixel or sets of pixels from each image across the entire energy range studied. EF-TEM images provide superior spatial resolution but can be difficult to analyse because of mode overlap over the energy window selected (typically 0.2 eV or higher). Not surprisingly, such electron microscopy-based techniques have gained tremendous popularity in the last decade;[85,118,119,121,122] their resolution improvements closely followed that of electron microscopes, in particular the implementation of aberration correction (both spherical and chromatic) and monochromation, such that this approach now has the highest routine spatial resolution of all near-field techniques.

Recent advances allowed the coupling of this powerful field mapping approach with tomography, aiming to reconstruct a 3-dimensional map by obtaining images at various tilt angles. Such experiments are expected to provide rich information on the fine details of plasmonic resonances in single and coupled particles.[123,124] Time-resolved experiments using pulsed electron beams may also become a reality in the near future.

As seen above, several techniques are available to probe the plasmonic behaviour of single metal nanoparticles, each with a different combination of spatial resolution, spectral resolution, expansion capabilities and ease of use and implementation. Such complementarity allows for the acquisition of a full spectrum of information on single particle optical behaviour. Upcoming developments are expected to improve the experimental throughput and render results more accurate and detail-rich.

3. New knowledge from single particle measurements

The tremendous advances in instrumentation described above, coupled with major synthetic breakthroughs, made many novel experiments possible in the last ten years. As a result, fundamental properties of plasmon resonances, such as their decay, dependence on structural factors, and near field distribution are now better understood. Applications such as particle tracking and nanosensing have also flourished, allowing the study of complex systems such as catalytic reactions and biological processes. In the following section, we will highlight several recent examples of fundamental studies and applications using single particle approaches to give the reader an exciting and up-to-date overview of the field.

3.1 Far-field spectroscopy studies of plasmonic behaviour

Tuning of the optical properties of metal nanoparticles can be efficiently achieved by controlling their shape and size. For example, the longitudinal LSPR resonance of Au rods of different aspect ratio can span the visible and near-IR spectrum,[32,77,125–127] while changing the size of Ag cubes from 50 to 200 nm (side length) shifts their dipolar resonance from approximately 450 to 800 nm.[128–130] Such tuning is essential for many applications where there exists an optimal plasmon resonance frequency, such as in surface-enhanced spectroscopies[58–60,131–135] and sensors based on molecular resonance coupling.[136,137]

The details of the size and shape dependence of the plasmon resonance energy and width are inherently blurred in bulk measurements because of the unavoidable inhomogeneity of colloidal reaction products. Single particle optical experiments, when coupled with structural information as described earlier in Section 2.1.5, provide a powerful approach to unravel the details of the structure–function relationships in plasmonic nanoparticles. Since the initial experiments of Mock *et al.*[138] showing large spectral differences between silver spheres decahedra, and triangles, single particle dark-field microscopy coupled with electron microscopy has been used on a large number of shapes such as triangles,[28,79,139,140] decahedra,[24,79] cubes,[73,74,80] cages,[141] spheres,[29,142] shells,[143] and rods.[25,77] In the studies mentioned above, single particle approaches uniquely characterized and quantified the effects of size and shape on the plasmonic behaviour of nanoparticles, and allowed the study of properties inaccessible with bulk measurements, such as plasmon decay and polarization effects. Recent examples highlighting these unique capabilities are presented below; additional discussion and review of earlier work can be found elsewhere.[83,139]

3.1.1 Quantitative effects of size and shape on plasmon energy and intensity. Shape and size are well known to influence LSPR behaviour, however only recently quantitative information suitable to provide valuable guidance for application development has appeared. Tcherniak *et al.*[29] have measured, using a combination of dark-field microscopy, PHI and SEM, the exact scattering/absorption ratio for the dipolar resonance of Au spheres. Their results are in perfect agreement with predictions from Mie theory and directly impact fields where Au nanoparticles act as photothermal devices. Quantitative plasmon energy and linewidth size-dependence characterization has been performed for sharp Au cubes, decahedra, icosahedra, triangles, and octahedra, such that the influence of shape on size effects was extracted.[79] The change in dipolar plasmon energy for a given size increase was found to be constant for all shapes when the dipolar resonance pathlength was used as the size parameter (the distance between poles of opposite charge); the simplicity of this dipolar behaviour provides tremendous predictive power for the size-dependence of arbitrary shapes. Going beyond dipolar resonances, single particle spectroscopy

uniquely allows accurate characterization of higher order modes often ill-separated in bulk spectra. The quadrupolar resonance of Ag cubes was characterized[73–75] and its size-dependence was found to be significantly smaller than that of the dipolar resonance,[73] as predicted by numerical simulations.[144] Recently, Wei *et al.* characterized size effects on the plasmon resonances in nanorice, a quasi-one-dimensional structure capable of supporting modes up to $l = 4$.[145–147] As seen in Fig. 4, plasmon energy size-dependence is very linear and less pronounced for higher order modes. In this study, the width of the particles was fixed at 60 nm, such that a single structural parameter, the length, could be isolated and varied over the range 200–600 nm; excellent agreement with boundary element method (BEM) results was obtained. Single particle studies can also quantitatively probe the effect of simultaneous structure and size effects as was performed for Ag–AgO shells[148] and Ag bipyramids.[149] In such cases multiparameter fits must be used, requiring large data sets. With the development and improvement of high throughput single particle approaches (wide field, ultramicroscopy, *etc.*), more such studies are likely to appear.

3.1.2 Size and shape effects on plasmon polarization. Far-field plasmon polarization, which reveals mode symmetry as well as particle anisotropy and orientation, can efficiently be probed by single particle approaches as they overcome the random orientation of bulk samples. Polarization-dependent spectra from an ensemble of templated or oriented particles can be obtained;[150] however, single particle spectroscopy can uniquely provide quantitative information on the magnitude of the intrinsic polarization-induced scattering intensity variation and mode selectivity. By combining dark-field microscopy with a variable wavelength interference filter and a rotating polarizer, a technique referred to as RotPol, Schubert *et al.*[26] probed the scattering of single Ag and Au nanoparticles and particle pairs as illustrated in Fig. 5. The polarization anisotropy for Au rods was found to vary as a function of rod resonance wavelength, a result in agreement with numerical calculations; these rods could be monitored during overgrowth to rounder particles, a process leading to a gradual decrease in resonance wavelength and polarization anisotropy. The authors also reported strong plasmon polarization for Ag triangles and Au sphere dimers, and observed no polarization for Ag cubes. Recent results confirm the latter in dark-field optical microscopy; however, when probed by scanning photoionization microscopy (where the cube absorbs 4 photons and emits an electron), a strong polarization dependence was observed.[80] Correlated structural measurements confirmed that the photoemission was enhanced when the laser polarization was aligned with the cube corners, strongly supporting coherent multiphoton photoelectron emission as the mechanism responsible for electron emission from Ag nanoparticles and ruling out thermionic and incoherent pathways.[80]

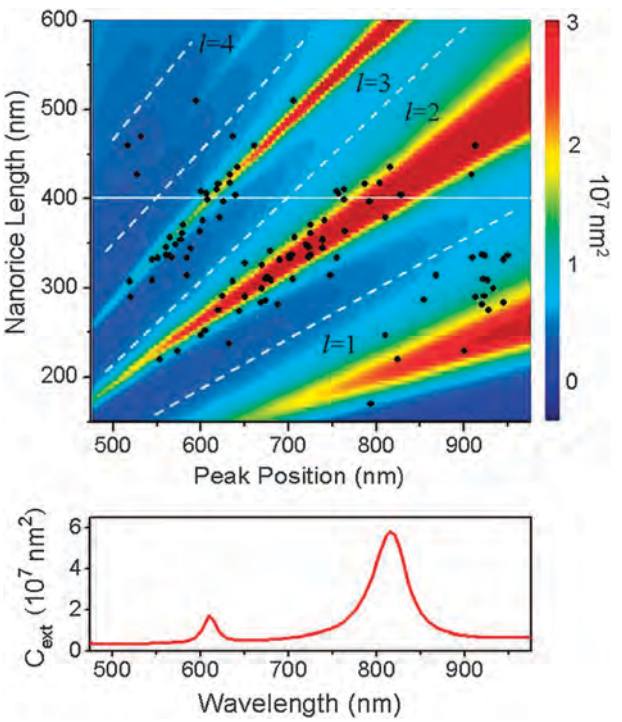

Fig. 4 Size dependent far-field response of Au nanorice. Top: peak position relationship to particle length, where the black dots are experimental scattering data from correlated dark-field microscopy and scanning electron microscopy, and the coloured background is boundary element method results for the extinction cross-section of 60 nm diameter particles. Bottom: extinction coefficient calculated for a nanorice with length of 400 nm (white line in top panel). Reproduced with permission from ref. 147.

Polarization effects can also be observed by incorporating a polarizer in the beam path of a dark-field setup, either before[82] or after the sample.[30] Using the latter, Nehl *et al.* studied the rather complex behaviour of Au stars and correlated the orientation of most intense scattering with the position of large protrusions.[30] Using the former, the scattering intensity for the lowest energy mode (longitudinal) of rods and linear sphere assemblies was found to peak when the polarization is aligned along the long axis.[77,82]

3.1.3 Refractive index sensitivity of single nanoparticles. A prominent feature of small metal particles is their nanosensing capabilities enabled by the sensitivity of their plasmon resonance energy to the surrounding medium. Small changes in size and shape strongly influence the refractive index sensitivity (RIS), such that single particle studies can uniquely provide insight and quantitative relationships between structural factors and sensing performance. Early studies by Mock *et al.* on random colloids[138,151] demonstrated a large (factor of 1.5) variation in RIS from particle to particle. While no direct structural correlation was performed, it was inferred from previous scattering data that the RIS increased from spheres to triangles to rods. Work by Sherry *et al.*[75,152] further showed that RIS can vary nearly as much for particles with nominally similar shapes and plasmon resonance frequencies, highlighting the importance of minute changes in size and corner rounding. Such acute dependence could be characterized quantitatively *via* correlated single particle RIS measurements and structural characterization, a difficult yet achievable experiment.

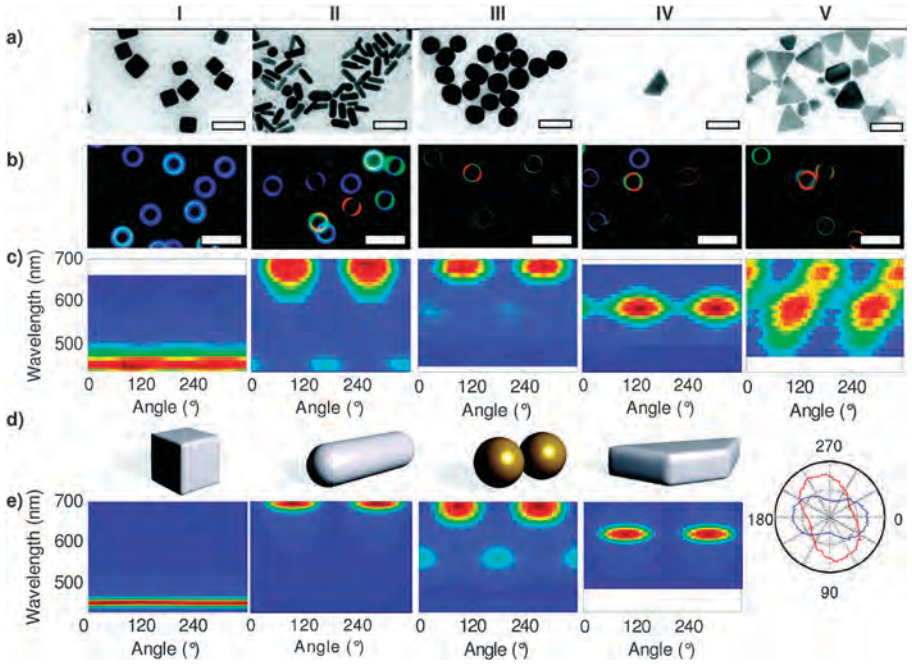

Fig. 5 Plasmon polarization results for single Au and Ag nanoparticles. (a) Representative TEM images of Ag(I, II, IV, V) and Au(III) structures. Scale bars, 100 nm. (b) Real-colour images obtained in the RotPol setup. Scale bars, 15 μm. (c) Representative polarization-dependent scattering spectra obtained for single nanostructures. (d) Shape models. (e) Computational results from discrete dipole approximation. Bottom right: polar graph of the scattering intensity from a triangular particle as a function of polarization showing a two-lobe pattern with 60° offset. Reproduced with permission from ref. 26.

3.1.4 Plasmon decay. The advantages of single-particle over bulk measurements so far emphasized have been mostly focused on the removal of the ensemble size distribution contribution. Yet additional information on plasmon decay can be gained by implementing single particle approaches. Plasmon lifetime is the result of several contributions from both radiative (effects such as finite volume, sharp-tip broadening, particle–substrate interactions) and nonradiative damping (intrinsic effect related to the loss in electric field strength in the metal dielectric function). The study of Rayleigh scattering is suitable for larger NPs for which plasmon damping, particularly retardation effects, appear. Sönnichsen *et al.* were the first to examine plasmon damping in single Au rod by dark-field microscopy.[77] A later study by Novo *et al.*[25] of more diverse rods used a similar technique to demonstrate that depending on the aspect ratio (and volume) of the rods, the prevailing plasmon decay mechanism is either electron scattering (small rods) or radiative damping (large rods). Other studies confirmed that electron-surface scattering effects become important whenever nanoparticles have one dimension (thickness for boxes and prisms, width for rods) smaller than ~10 nm.[25,28,141] Several larger nanoparticle systems dominated by radiation damping dominates, have been examined by dark-field microscopy, including Au spheres,[77] Au rods,[77] Ag triangular prisms,[28,140] Au decahedra,[24,79] Au truncated bitetrahedra,[79] Au cubes,[73,79] Au icosahedra,[79] Au octahedra,[79] and Ag–Au boxes.[141]

From these studies, it appears that a dramatic reduction in the linewidth should be available in systems with a large electron mean free path and low radiative damping. Single particle studies can unravel what environmental factors (substrate, surrounding solvent, *etc.*) and particle geometry (shape, truncation, thickness, *etc.*) provide the most powerful handles to manipulate plasmon decay. For example, radiative damping was shown to be lower in slightly truncated particles (*vs.* sharp ones) and in nanoparticles sufficiently large to yield a large electron mean free path.[28] However, lateral dimensions and volume must be kept low to minimize radiative damping. Given some experimental interpretation difficulties and the limited data sets typically available, coupling single particle studies with computational approaches, as was done recently by Blaber *et al.*,[28] provides additional insight on plasmon decay. Indeed, comparison between electrodynamics results and experimental data on the plasmon decay of thin platelets unravelled a likely plasmon path along the longitudinal axis, *i.e.* in the plan parallel to the nanostructure long axis.[28] Larger and more sophisticated data sets coupled with similar numerical approaches are expected to further enrich the knowledge on decay lifetime by surmounting the difficulties associated with the larger particle to particle variability present in lifetime analysis when compared to plasmon energy (λ_{max}) analysis.

3.2 Near-field effects and their dependence on particle size, shape, and aggregation state

3.2.1 Plasmons probed in the near-field. As seen above, single particle far-field approaches can be used to extract rich information on the structure–function relationships in plasmonic nanoparticles, ranging from refractive index sensitivity to scattering and absorption properties, polarization effects, and plasmon decay. However, such measurements indirectly probe the underlying electron oscillation phenomenon. With near-field techniques,

electric field potential maps providing the details of the electron resonance pattern can be obtained. Shape effects can thus be visualized directly as different geometric distribution of the electric field potential in and around the particle. This is of particular interest for fundamental studies on plasmonic behaviour as well as in the optimization of substrates for surface-enhanced spectroscopies. Indeed, as will be discussed later, the regions of high field intensity are believed to provide most of the signal enhancement in, for example, SERS,[48,51,153–156] such that quantifying the intensity and size of such "hot spots" is of critical importance. Any of the techniques described in Section 2.2 can be used to produce such electric field maps, with various levels of resolution (Table 1). Note that there exists a growing discussion about the exact nature of the observed signal in near-field approaches.[157,158] However this section will focus on two prominent types of information uniquely obtained by near-field techniques; the reader is referred to recent reviews for further and more specialized discussion.[92,139,159]

Amongst the unique aspects of plasmonic behaviour that can be probed in the near-field are ultralocal variations of the electric field due to differences in corner sharpness within the same particle. Indeed, large changes in field intensity at the tips of Ag triangles and cubes have both been observed. EELS studies of the former showed that a higher corner angle (larger radius of curvature) leads to lower field concentration: the 76.5° corner had the weakest interaction with the electron beam, followed by the shaper 59.5° and 44° corners.[119] Similar effect were observed and calculated for cubes, in which the absorption resonance at different corners was found to be mostly independent of each other and rather be dictated by the local shape and environment.[121]

Another unique capability of near-field approaches is the possibility to gain profound understanding of high order (high energy) modes, for which the field distribution is not as obvious and symmetric as for dipolar modes. Such plasmon resonances can be visualized by observing the electric fields around a particle at a specific, narrow energy range such that the overlap from other modes is minimized. Exquisite detail can be obtained using energy-filtered TEM imaging; a recent example in Fig. 6 shows the field distribution for the $m = 1$ to $m = 6$ modes in a Ag rod.[120] Similar results have been obtained, albeit with much more limited spatial resolution, using cathodoluminescence[160] and two-photon-induced luminescence.[101,161] Near-field mapping also provides access to "dark modes", *i.e.* modes which cannot be excited in the far field because of their lack of net dipole moment. Koh *et al.*, for example, recently used STEM-EELS to probe the plasmon modes in fabricated nanoantennas made of one to three triangular structures, revealing both dark and bright modes within their rich coupling patterns.[85]

3.2.2 Field enhancements studies from far-field spectroscopy. Studies correlating near-field and/or far-field microscopies (including TEM, SEM, AFM, and LSPR imaging) with SERS and other enhanced spectroscopies have allowed for interrogation of the effect of nanoparticle shape and aggregation on field intensity. "Single" particle SERS is somewhat of a misnomer, as it is generally agreed that most monomer nanoparticles do not provide sufficient EFs ($>10^4$).[162] Generally, "single" particle SERS involves dimers, trimers, and higher order aggregates, either bare or coated with silica, to provide the hot spots necessary for generating significantly enhanced electromagnetic fields.[156,163,164] From studies of dimers and trimers of 150 nm spheres, it was found that EFs do not correlate with aggregation state. Instead, only a single hot spot seems necessary for significant enhancement.[156,164] It was also found, as shown in Fig. 7, that there is no direct correlation

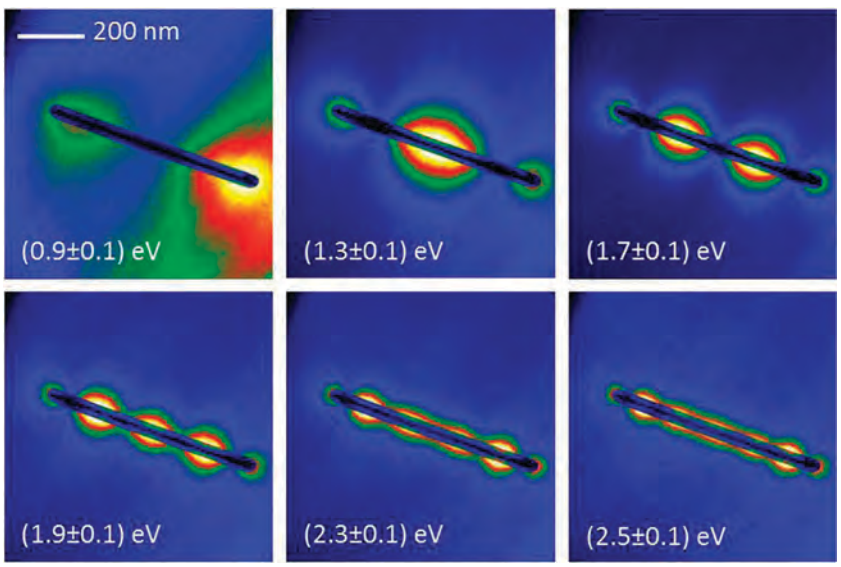

Fig. 6 Energy-filtered transmission electron micrographs of a single Ag rod obtained in a monochromated Zeiss SESAM FEG-TEM operated at 200 keV with an energy selecting slit of 0.23 eV. Modes from the fundamental ($m = 1$) to the $m = 6$ mode are clearly visible. The intensity of the energy-loss maps is shown as a temperature colour scale. Reproduced with permission from ref. 120.

between the LSPR λ_{max} (a far-field effect) and the SERS maximum EF (a near-field phenomenon) when the system is hot spot dominated.

Recent advances in nanoparticle synthesis has resulted in increasingly successful attempts to create hot spots in single nanoparticles by synthesizing shapes with extremely sharp features, including stars,[165] spiked gold beads,[166] cubes,[167,168] and octopod structures.[168] Fig. 8a shows a Raman signal map overlaid on the corresponding SEM image, confirming the single particle origin of the signal. Fig. 8b shows an example of the Raman spectra used to generate the map, clearly showing that the highest signal intensity is obtained with the etched octahedral particles.[168] The authors also tested the wavelength dependence of the enhancement produced by their particles, and found that compared with excitation at 514 nm, the mildly etched particles had a higher SERS signal intensity at 633 nm, while the octopod particles demonstrated a higher intensity at 785 nm, with EFs $\sim 5 \times 10^5$, *i.e.* an order of magnitude better than most monomers. To date, the best effort for achieving highly enhancing single particle SERS utilized LSPR spectroscopy, high resolution STEM, EELS, SEM and SERS, to demonstrate that attaching single Au stars to surface-bound 1,5-naphtalenedithiol molecules formed intense hot spots between the nanostar tips and the optically thick Au substrate. The low concentration of molecules on the surface insured that only one or two molecules would reach the hot spot, such that the EFs calculated for the stars were on the order of 10^{10}, three orders of magnitude higher than for dimers of spheres (EFs $\sim 10^7$).[165] An important issue to note is that nanoparticles such as stars, cubes and triangles, all with sharp corners, as well as rods, are more highly sensitive to polarization orientation than more truncated structures.[167,168] Thus, when performing single particle SERS measurements with non-spherical structures, it is critical to take laser polarization into account.[164,167,169] Such studies indicate the possibility of achieving highly enhancing structures for true single particle SERS, given the appropriate nanoparticle geometry and laser polarization.

Another approach to probing the electric field on nanoparticles, second harmonic generation (SHG) imaging, has been used to characterize type I collagen fibres in extracellular matrices, connective tissue, and internal organs.[62] Generally in SHG, spherical nanoparticles are more easily observed as trimers than dimers because of symmetry, although if the particles are not spherical dimers and trimers have comparable activity.[63] Jin *et al.*[63] showed that SHG is symmetry forbidden for bulk samples such as silver due to the inversion symmetry in bulk silver. It is, however, possible for SHG at the single silver particle level, due to both the surface contribution, and the enhancement from the plasmon resonance. Indeed, excitation along the longitudinal axis of the rods created the SHG response through nonlinearity in the polarization.[63] Because SHG can be used to interrogate the nonlinear properties of nanoparticle systems and is sensitive to polarization effects at the single particle level, it is expected to evolve as an important tool in nanotechnology.

3.3 Monitoring chemical and biological processes with the plasmonic response of single nanoparticles

As previously illustrated in this paper, monitoring the shift in λ_{max} of a nanoparticle is a relatively easy way to measure changes of the nanoparticle itself (size and shape) or its

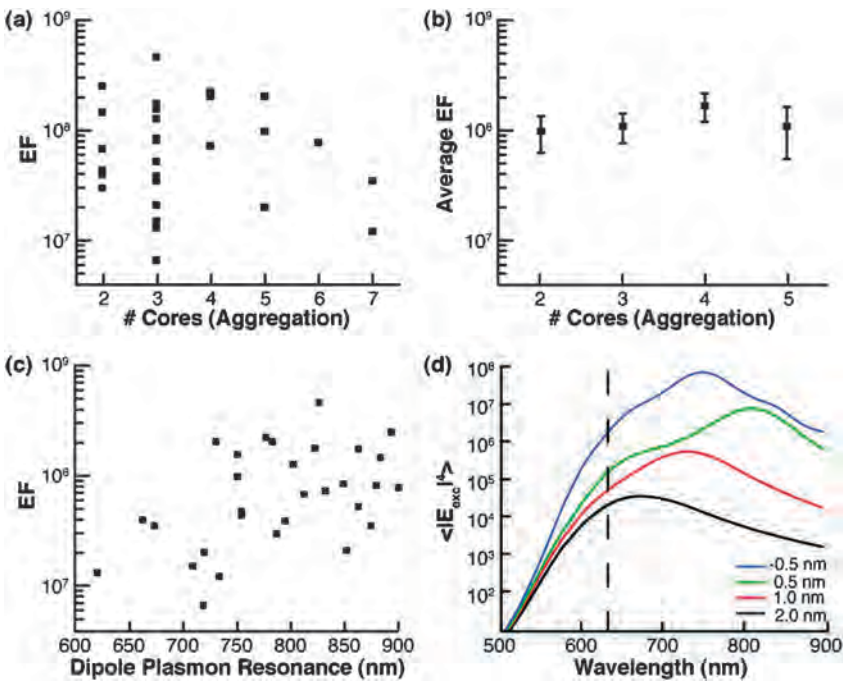

Fig. 7 (a) SERS enhancement factors (EFs) for 30 single Au sphere aggregates as a function of number of cores. (b) Average EF for each number of cores show constant behavior regardless of the number of hot spots present. (c) Lack of correlation between EF and dipole plasmon resonance energy. (d) Calculated $\langle |E_{exc}|^4 \rangle$ for a dimer structure as a function of the interparticle separation; at λ_{ex} = 633 nm, the average EM enhancement increases by $\sim$2 orders of magnitude with decreasing gap size. Reproduced with permission from ref. 156.

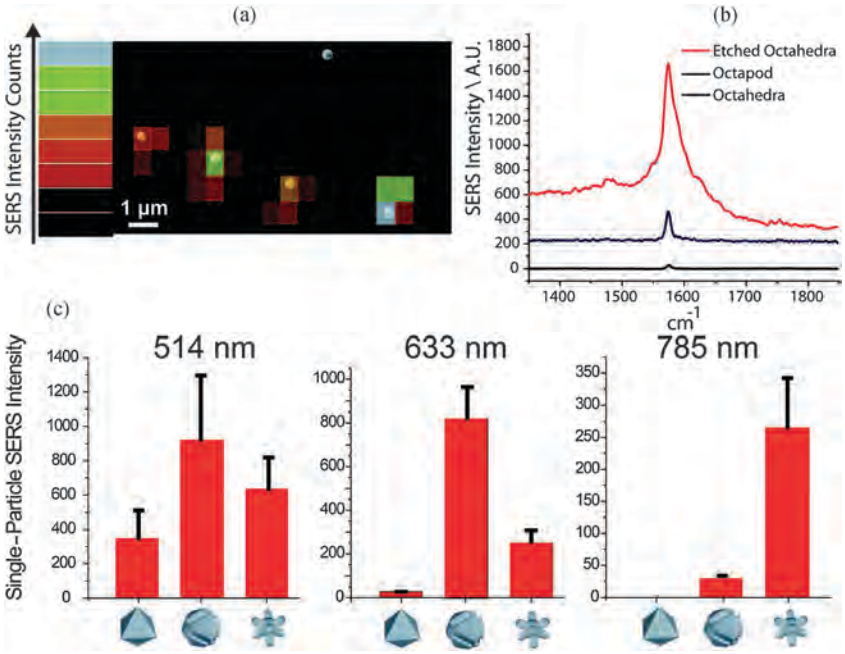

Fig. 8 Surface-enhanced Raman scattering of benzenethiol on single Ag nanoparticles. (a) SEM image of particles overlaid with SERS intensity map of the 1584 cm^{-1} mode of benzenethiol. (b) SERS spectra for each shape particle obtained with 633 nm excitation. (c) Average single particle SERS intensity as a function of shape and excitation wavelength. Reproduced with permission from ref. 168.

surrounding environment, even allowing the tracking of chemical events at the surface of single particles *via* dark-field microscopy or photothermal imaging. The potential for monitoring surface binding events is of great interest for fields such as catalysis, materials science, biology, and biochemistry, such that many exciting new developments have emerged recently; we highlight some of the most important ones below.

Nanoparticle oxidation can be tracked optically using their plasmonic signature. Oxidation of Cu has been observed on triangular nanoparticle arrays fabricated by nanosphere lithography[170] and more recently continuously monitored in real time at the single nanoparticle level by dark-field microscopy.[171] Cheng *et al.* were able to identify heterogeneous reaction pathways and intermediate states of the oxidation kinetics of cetyltrimethylammonium bromide (CTAB)-coated Au rods by H_2O_2 in the presence of Br[172] by studying single particle scattering with dark-field microscopy. They found that mild oxidation happens likely at the tips of the rods (where the CTAB capping layer is less dense) resulting in a shortening of their length well matching the observed blue-shift of the longitudinal LSPR peak. By monitoring heterogeneous reaction rates as well as reaction pathways, a self-catalysis mechanism previously hindered by ensemble-averaged measurements was revealed. Alternatively, it is possible to externally control the plasmonic signature by applying an electrochemical potential; the colour change is visible in dark-field microscopy.[173] The amplitude of the spectral shifts was observed to vary with the particle morphology, being most influenced by the presence of tips or any other electromagnetic field hot spots that are expected to have higher rates of electron transfer. Colour changes in Au rods were of such magnitude to be observable by eye when the potential was stepped from −1.0 V to −1.6 V (Fig. 9).

Direct observation of chemical reactions on single Au particles by dark-field microscopy was first reported by the Mulvaney group.[174] By correlating the shift in LSPR λ_{max} and the change in the nanoparticle electron density, they achieved a quantitative description of Au-catalysed oxidation of ascorbic acid by dissolved oxygen at the nanoparticle surface. More specifically, the resonance shift observed for one nanoparticle in one redox cycle can be related to the number of O_2 molecules involved in the reaction per second, given knowledge of the number of atoms in the structure (volume derived from TEM images) and the reaction stoichiometry. Ultimately, this study demonstrated another great application of dark-field

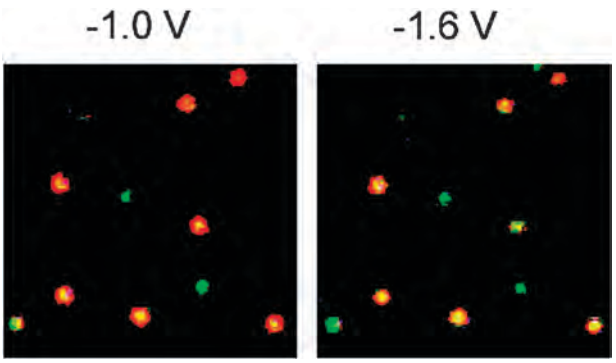

Fig. 9 Real colour image from dark field microscopy showing the electric potential induced shift in scattering λ_{max} for single Au nanoparticles (red = rods, green = spheres or triangular prisms). Reproduced with permission from ref. 173.

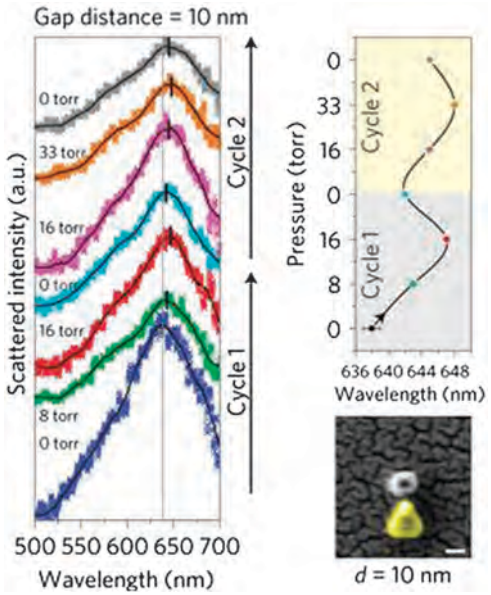

Fig. 10 Antenna-enhanced hydrogen sensing using a Au triangular platelet and a Pd nanoparticle separated by a 10 nm gap. The left diagram shows the scattering spectrum of the nanoantennas for the different hydrogen pressure values; the hydrogen partial pressure is raised first from 0 Torr to higher pressures (cycle 1) and then driven back to 0 Torr (cycle 2). The right diagram shows the behaviour of the resonance peak on hydrogen cycles 1 and 2. An SEM image of the nanostructure is shown in the lower right. Scale bar, 50 nm. Reproduced with permission from ref. 176.

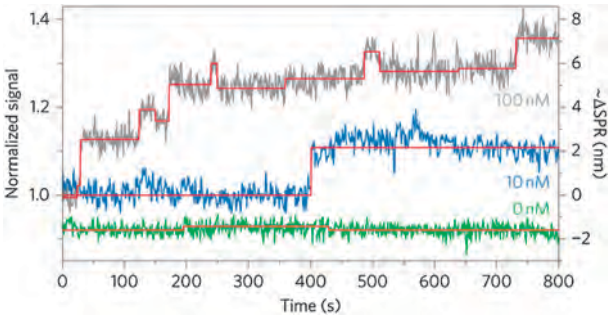

Fig. 11 Time trace of normalized photothermal signal and relative LSPR shift for biotin-functionalized single Au rods in the presence of different concentrations of a streptavidin–R-phycoerythrin conjugate. Because of the single wavelength measurement performed, the right-hand axis corresponds to an estimate of the LSPR redshift deduced from the linewidth of the individual rods. Reproduced with permission from ref. 10.

microscopy, namely its capability to directly quantify redox reactions in plasmonic nanoparticles.

Other chemical reactions have since been monitored, such as the generation of hydrogen by photodecomposition of lactic acid at the surface of cubic particles made of platinized cadmium sulfide with gold cores (Au@Pt/CdS) by dark-field microscopy.[175] Hydrogen detection was also central to a study by Liu *et al.*,[176] which monitored indirectly the change induced by the adsorption of hydrogen molecules on Pd posts located 10 to 50 nm apart from a single Au triangle or rod. While Pd greatly absorbs hydrogen, it is a weak plasmonic material such that a broad and damped scattering spectrum is observed both in the presence and absence of hydrogen. In the close presence of Au, however, a nanofocusing effect (optical nanoantenna effect) increases the λ_{max} shift of the Pd nanoparticle, as illustrated in Fig. 10. Such robust plasmonic detection of a low-mass gas demonstrates that nanoantennas based on the controlled assembly of nanoparticles are promising for molecular sensing and single-molecule detection.

Single molecule detection, the ultimate sensitivity limit, has recently been demonstrated for plasmonic systems *via* the adsorption of large single proteins (with molecular weight above 53 kDa) at the surface of single Au rods. This experiment was rendered possible by clever, tip-specific functionalization of the particles with receptors. In this study by Zijlstra *et al.*,[10] the shift of the longitudinal surface plasmon resonance at a single frequency was monitored by photothermal imaging. The single-molecule nature of the binding events is illustrated in Fig. 11, where the normalized photothermal signal and relative plasmon resonance frequency shift is reported over a 800 s period during which the protein (streptavidin–R-phycoerythrin conjugate) is put in the vicinity of the nanoparticle. Interestingly, the approach of molecules that leave the probing volume within tens of seconds can be observed. Method generality was established by probing three different biotin-binding proteins (streptavidin, antibiotin, and a streptavidin–R-phycoerythrin conjugate) as well as different single rods. The Sönnichsen group also reported single-molecule adsorption events on a single plasmonic sensor. Using a dark-field optical microscope equipped with a white light laser source and intensified CCD camera detector, they monitored the LSPR λ_{max} shift in the scattering spectrum of single Au rods induced by the binding of fibronectin.[7] Single Au rod scattering spectra could be obtained within a few milliseconds with an impressive spectral resolution of 0.03 nm (after fitting the spectral resonance). The simple structure of both sensors (single nanoparticle) makes such approach attractive as it avoids any fabrication/assembly difficulties while reaching unprecedented detection capabilities.

3.4 Nanoparticle tracking

Dark-field microscopy is, as discussed in many parts of this article, a robust and flexible tool easily integrated in multi-component/multi-instrument studies. Because of its fast speed and high sensitivity to plasmonic scattering, it provides a unique and highly effective method for the investigation of the dynamic motion of nanoparticles under various, potentially complex conditions such as biological media. Combining LSPR imaging with a wavelength selector (liquid crystal tuneable filter), Bingham *et al.*[22] characterized the plasmonic response and motion of diffusing nanoparticles, and recorded the scattering of multiple ~35 nm Ag nanoparticles and ~100 nm Ag prisms in parallel. Such high-throughput method is extremely attractive for single particle studies as it provides LSPR information and diffusion coefficients simultaneously and in real-time.[22]

Using high speed video microscopy (video rate of 25 μs) and fluorescence, Fujiwara *et al.*[68] tracked a 40 nm Au nanoparticle functionalized with a lipid (1,2-dioleoyl-*sn*-glycero-3-

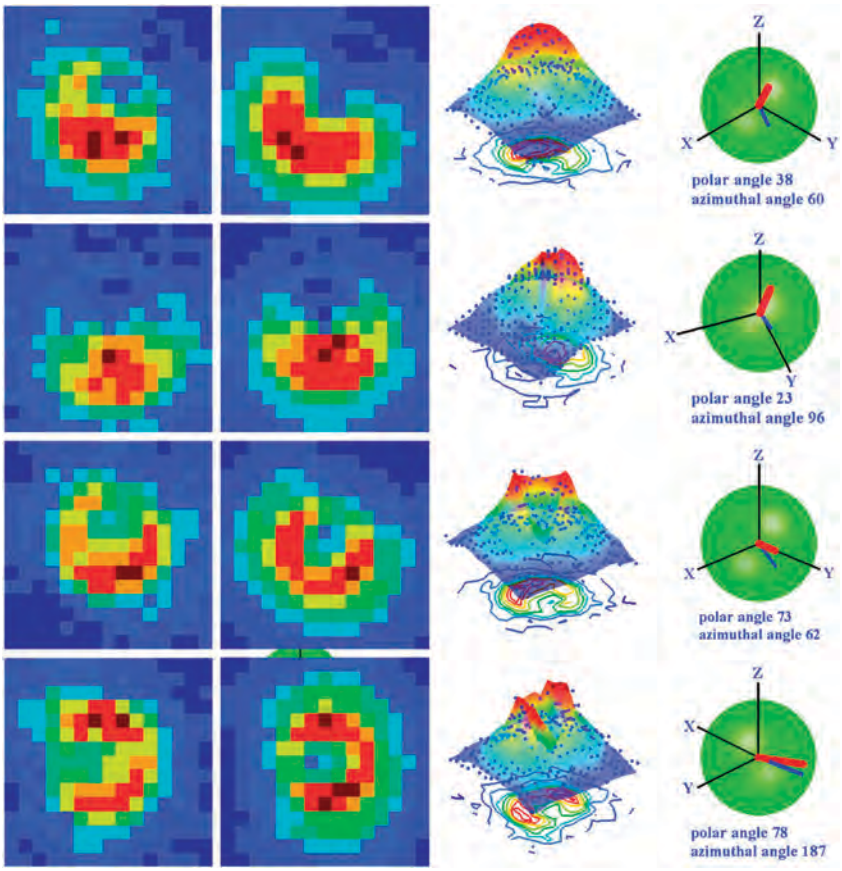

Fig. 12 Orientational mapping using dark field microscopy. Far left: measured dark-field images from four Au rods. Left: best-fit simulated dark-field images. Right: 3D intensity distribution plots including contour plots and blue dots representing measured values and showing good agreement with simulated data. Far right: 3D orientation models of the corresponding rods. Reproduced with permission from ref. 179.

phosphoethanolamine (DOPE)) in the cell membrane. They observed that the cell membrane is compartmentalized with respect to lateral diffusion of phospholipids. This compartmentalization confines the nanoparticle–DOPE complex within a compartment, limiting long-range diffusion. Actin-based membrane skeleton, regulating membrane compartment boundaries, was thus involved in the process, a finding supported by the simple Brownian diffusion of the nanoparticle–DOPE complex in areas of the membrane where the skeleton was found to be depleted. Other studies involving membranes include that of the rotary molecular motors comprising F_0F_1 ATP synthase with Au rods.[70] Unlike single molecular Förster resonance energy transfer or attaching actin filaments or nanoparticles to the rotor, *i.e.* techniques which are hampered by limited time and angular resolution as well as having long acquisition times, dark-field microscopy combined with polarization effects allows for shorter data acquisition times, improved time resolution (5 μs), and a superior signal-to-noise ratio. This time resolution and signal intensity resulted in the elucidation of the F_0 Brownian ratchet mechanism, as well as the observation of transient dwells from interaction between the F_0 rotor and the F_0F_1 complex.

Rods are prominent in tracking studies because polarized light can give information about their orientation. Sönnichsen *et al.*[33] utilized this feature to track the 2D orientation of Au rods confined at a glass–water interface. The fastest rotational diffusion times recorded were ~60 ns, with the local viscosity dominated by particle–surface interactions. They also found that some particles were "sticky" (attaching to the surface) and hence had longer diffusion times.

The tracking of nanoparticles quickly became of interest to *in vivo* studies because of the widespread possible applications in live cells such as biosensing, drug delivery, diagnostics, and therapeutics.[65,177] Indeed, nanoparticle tracking combines the advantages of single particle and single molecule tracking, namely the unlimited observation time due to lack of photobleaching and the absence of disruption to the surrounding environment due to the small size of the marker. Absorption-based imaging (LISNA) allowed for 2D tracking of 5 nm Au spheres in the planar membrane of live cells,[40] yielding information about the protein lateral diffusion at greater signal intensities than with fluorescence. Utilizing a fs white light continuum with dark-field microscopy, Louit *et al.*[71] monitored the interaction of 80 nm Au spheres with living mouse fibroblast cells, observing diffusion of ~5 μm over an hour time period. Changes in the particle scattering maximum position and intensity of interferences correlated with exo- and endocytotic processes: changes in nanoparticle height of 1–2 μm within the cell

along with increased cell background signal and interferences were indicators of the nanoparticle undergoing endocytosis, providing a tool to track such interactions.

Beyond membrane diffusion and cytosis, nanoparticles tracking can unravel details about intracellular transport. Incorporating a quadrant photodiode and a feedback-looped piezo stage (to maintain position) to dark-field microscopy, Nan *et al.*[178] resolved individual steps of the molecular motors kinesin and dynein using 100–150 nm Au nanoparticles functionalized with human fibroblast growth factor in lung cancer cells. The time resolution of $\sim$25 μs was limited by particle size (smaller particles would result in decreased time resolution), and the spatial resolution was $\sim$1.5 nm, an unprecedented result which allowed for the detection of individual motion steps at full range *in vivo* velocities (0–8 μm s^{-1}).

Finally, moving towards 3D particle tracking, Xiao *et al.*[179] used a defocused approach, where they introduced an aberration into the dark-field imaging of Au rods. By interpreting the electric field distribution pattern, the orientation angle of the oscillating dipoles of the individual rods was resolved, resulting in spatial information about the Au rods (Fig. 12).[65,179]

4. Challenges, open questions, and future directions

Single particle approaches have shown to be a powerful tool in fundamental studies and are gaining momentum as part of devices and sensing technology owing to their multiplexing capabilities and small sensing volume. Several areas benefited from the recent instrumental advances in single particle studies described in Section 2, yet many open questions and challenges remain, in particular in novel nanoparticle architectures, single molecule sensing, and *in vivo* studies.

Single particle studies of the dynamics of (bio)chemical and catalytic reactions offer a unique way to unobtrusively probe an extremely small volume. However, to obtain strong signals, understanding, control, and optimization of particle geometry is paramount. Many exciting synthetic advances have been reported; now the challenge lies in the successfully transition from making to using such novel particles. Complex, multifunctional architectures such as bimetallic particles represent one such class of materials ripe for single particle studies and application implementation. A recent example is the Au@Pd–Au octopodal structure, which could provide exquisite tracking and perhaps even optical control of Pd-catalysed chemical reactions at the single particle level.[180,181] Such bimetallic structures also widen the spectrum of available attachment chemistry beyond the traditional Au–thiol architecture. Advances in control of nanoparticle assembly should also provide novel single particle (rather single assembly) sensing platforms. For example, strong interactions between quadrupolar modes in a 3-D plasmon ruler[182] consisting of a Au rod sandwiched between two pairs of parallel Au rods in a ''H'' shape produces sharp spectral features allowing for a large increase in the sensing figure of merit (*via* its 1/FWHM dependence). These unique spectral features are directly correlated with the 3D configuration of the Au rods, such that the smallest change in their relative position produces a clear signal which could be used to quantify molecular structure changes given appropriate calibration, with potential applications in the study of macromolecules dynamics and other biological processes.[182] Mode hybridization shows promises as a powerful sensing platform that is not confined to the hybridization of similar modes, as demonstrated by the coupling of single particle and microcavity modes by Schmidt *et al.*[183]

The interest in single molecule spectroscopy has fostered a large body of research in the last ten years, mostly at the proof-of-concept level, yet the field is still far from generalized, reproducible, and robust single molecule sensing. A limited number of reports, discussed above, claim single molecule detection from LSPR spectroscopy, while single molecule SERS has become a well-established field.[59,60,184–187] For the latter, more robust single molecule SERS substrates are expected to emerge from the powerful design rules gained from a better understanding of the hot spot phenomenon.[48,49,51,153–155] The advancement and practical implementation of the former relies on a combination of improved particle design and instrumental advances, moving forward refractive index sensitivity as well as energy resolution.

Single particle plasmonic sensors have been demonstrated to be efficient at not only label-free single-molecule detection but at monitoring real-time adsorption and desorption events happening at their surface. The specificity of such events can be tailored *via* surface functionalization, a concept critical to biocompatibility and many sensing approaches.[188–190] Plasmonic sensors indeed have a very promising future as intracellular probes for monitoring dynamic biochemical processes within cells and thermodynamics of small systems. The versatility of the single plasmonic sensors, *e.g.* relative ease to fabricate nanoparticles such as rods in a controlled manner, enables *in vivo* studies aiming not only at monitoring intracellular chemical reactions, but how those 'nanobeacons' affect their living host, *i.e.* the associated nanotoxicology. Nanoparticles can also act as mechanical probes for investigating the environment they are embedded in. By monitoring their scattering spectrum over time it is possible to calculate their associated diffusion coefficient, as was recently done in transmembrane glycolipid, for example.[69]

It is no doubt that the wide diversity of far-field and near-field techniques offered for the study of the fundamental to applied plasmonic behaviour of metal nanoparticles represents a tremendous opportunity for fundamental plasmonic studies as well as sensing and device application. Furthermore, the implementation of multi-technique correlated studies on single plasmonic nanoparticles has allowed for understanding the structure–function and inter functions relationships in those systems.

Acknowledgements

This work was supported by the National Science Foundation (NSF CHE-0911145, CHE-1152547, DMR-1121262) and by

DARPA under SSC Pacific grant N660001-11-1-4179. Any opinions, findings, and conclusions or recommendations expressed in this publication are those of the author(s) and do not necessarily reflect the views of DARPA. E.R. acknowledges support from Northwestern University in the form of a presidential fellowship.

References

1 M. Faraday, *Philos. Trans. R. Soc. London*, 1857, **147**, 145–181.
2 G. Mie, *Ann. Phys.*, 1908, **25**, 377–445.
3 S. Weiss, *Science*, 1999, **283**, 1676–1683.
4 G. V. Hartland, *Annu. Rev. Phys. Chem.*, 2006, **7**, 403–430.
5 R. Vogelgesang and A. Dmitriev, *Analyst*, 2010, **135**, 1175–1181.
6 S. A. Maier, *Plasmonics: Fundamentals and Applications*, Springer, New York, 2007.
7 I. Ament, J. Prasad, A. Henkel, S. Schmachtel and C. Sönnichsen, *Nano Lett.*, 2012, **12**, 1092–1095.
8 D. Boyer, P. Tamarat, A. Maali, B. Lounis and M. Orrit, *Science*, 2002, **297**, 1160–1163.
9 C. L. Wong, G. C. K. Chen, B. K. Ng, S. Agarwal, N. Fanani, Z. Lin, S. Vasudevan and P. Chen, *Opt. Eng.*, 2011, **50**, 073201–073201.
10 P. Zijlstra, P. M. R. Paulo and M. Orrit, *Nat. Nanotechnol.*, 2012, **7**, 379–382.
11 S. Berciaud, L. Cognet, G. A. Blab and B. Lounis, *Phys. Rev. Lett.*, 2004, **93**, 257402.
12 P. Billaud, S. Marhaba, N. Grillet, E. Cottancin, C. Bonnet, J. Lermé, J.-L. Vialle, M. Broyer and M. Pellarin, *Rev. Sci. Instrum.*, 2010, **81**, 043101.
13 K. Imura and H. Okamoto, in *Progress in Nanophotonics 1, Nano-Optics and Nanophotonics*, ed. M. Ohtsu, Springer-Verlag, Berlin, Heidelberg, 2011.
14 J. Lin, N. Weber, A. Wirth, S. H. Chew, M. Escher, M. Merkel, M. F. Kling, M. I. Stockman, F. Krausz and U. Kleineberg, *J. Phys.: Condens. Matter*, 2009, **21**, 314005.
15 R. M. Tromp, J. B. Hannon, A. W. Ellis, W. Wan, A. Berghaus and O. Schaff, *Ultramicroscopy*, 2010, **110**, 852–861.
16 P. Chaturvedi, K. H. Hsu, A. Kumar, K. H. Fung, J. C. Mabon and N. X. Fang, *ACS Nano*, 2009, **3**, 1965–2974.
17 F. J. García de Abajo, *Rev. Mod. Phys.*, 2010, **82**, 209–275.
18 R. F. Egerton, *Electron energy-loss spectroscopy in the electron microscope*, Springer, 2011.
19 R. Zsigmondy, *Nobel Lectures, Chemistry*, Elseiver Publishing Company, Amsterdam, 1966.
20 W.-S. Chang, L. S. Slaughter, B. P. Khanal, P. Manna, E. R. Zubarev and S. Link, *Nano Lett.*, 2009, **9**, 1152–1157.
21 K. Lindfors, T. Kalkbrenner, P. Stoller and V. Sandoghdar, *Phys. Rev. Lett.*, 2004, **93**, 037401.
22 J. M. Bingham, K. A. Willets, N. C. Shah, D. Q. Andrews and D. R. P. Van, *J. Phys. Chem. C*, 2009, **113**, 16839–16842.
23 A. D. McFarland and R. P. Van Duyne, *Nano Lett.*, 2003, **3**, 1057–1062.
24 J. Rodríguez-Fernández, C. Novo, V. Myroshnychenko, A. M. Funston, A. Sánchez-Iglesias, I. Pastoriza-Santos, J. Pérez-Juste, F. J. García de Abajo, L. M. Liz-Marzán and P. Mulvaney, *J. Phys. Chem. C*, 2009, **113**, 18623–18631.
25 C. Novo, D. Gomez, J. Perez-Juste, Z. Zhang, H. Petrova, M. Reismann, P. Mulvaney and G. V. Hartland, *Phys. Chem. Chem. Phys.*, 2006, **8**, 3540–3546.
26 O. Schubert, J. Becker, L. Carbone, Y. Khalavka, T. Provalska, I. Zins and C. Sönnichsen, *Nano Lett.*, 2008, **8**, 2345–2350.
27 P. Zijlstra, J. W. M. Chon and M. Gu, *Phys. Chem. Chem. Phys.*, 2009, **11**, 5915–5921.
28 M. G. Blaber, A.-I. Henry, J. M. Bingham, G. C. Schatz and R. P. Van Duyne, *J. Phys. Chem. C*, 2012, **116**, 393–403.
29 A. Tcherniak, J. W. Ha, S. Dominguez-Medina, L. S. Slaughter and S. Link, *Nano Lett.*, 2010, **10**, 1398–1404.
30 C. L. Nehl, H. Liao and J. H. Hafner, *Nano Lett.*, 2006, **6**, 683–688.
31 M. A. van Dijk, M. Lippitz and M. Orrit, *Acc. Chem. Res.*, 2005, **38**, 594–601.
32 V. Myroshnychenko, J. Rodríguez-Fernández, I. Pastoriza-Santos, A. M. Funston, C. Novo, P. Mulvaney, L. M. Liz-Marzán and F. J. García de Abajo, *Chem. Soc. Rev.*, 2008, **37**, 1792–1805.
33 C. Sönnichsen and A. P. Alivisatos, *Nano Lett.*, 2005, **5**, 301–304.
34 K. A. Koen, M. L. Weber, K. M. Mayer, E. Fernandez and K. A. Willets, *J. Phys. Chem. C*, 2012, **116**, 16198–16206.
35 J. Lermé, G. Bachelier, P. Billaud, C. Bonnet, M. Broyer, E. Cottancin, S. Marhaba and M. Pellarin, *J. Opt. Soc. Am. A*, 2008, **25**, 493–514.
36 H. Baida, P. Billaud, S. Marhaba, D. Christofilos, E. Cottancin, A. Crut, J. Lerme, P. Maioli, M. Pellarin, M. Broyer, F. N. Del, F. Vallee, A. Sanchez-Iglesias, I. Pastoriza-Santos and L. M. Liz-Marzan, *Nano Lett.*, 2009, **9**, 3463–3469.
37 C. F. Bohren and D. R. Huffman, *Absorption and Scattering of Light by Small Particles*, Wiley, New York, Chichester, 1983.
38 M. A. van Dijk, A. L. Tchebotareva, M. Orrit, M. Lippitz, S. Berciaud, D. Lasne, L. Cognet and B. Lounis, *Phys. Chem. Chem. Phys.*, 2006, **8**, 3486–3495.
39 S. Berciaud, D. Lasne, G. A. Blab, L. Cognet and B. Lounis, *Phys. Rev. B: Condens. Matter Mater. Phys.*, 2006, **73**, 045424.
40 D. Lasne, G. A. Blab, S. Berciaud, M. Heine, L. Groc, D. Choquet, L. Cognet and B. Lounis, *Biophys. J.*, 2006, **91**, 4598–4604.
41 A. Arbouet, D. Christofilos, N. Del Fatti, F. Vallée, J. R. Huntzinger, L. Arnaud, P. Billaud and M. Broyer, *Phys. Rev. Lett.*, 2004, **93**, 127401.
42 S. Berciaud, L. Cognet, P. Tamarat and B. Lounis, *Nano Lett.*, 2005, **5**, 515–518.
43 C. Leduc, J.-M. Jung, R. R. Carney, F. Stellacci and B. Lounis, *ACS Nano*, 2011, **5**, 2587–2592.
44 A. Gaiduk, P. V. Ruijgrok, M. Yorulmaz and M. Orrit, *Chem. Sci.*, 2010, **1**, 343–350.

45 W.-S. Chang and S. Link, *J. Phys. Chem. Lett.*, 2012, **3**, 1393–1399.
46 O. L. Muskens, P. Billaud, M. Broyer, N. Del Fatti and F. Vallée, *Phys. Rev. B: Condens. Matter Mater. Phys.*, 2008, **78**, 205410.
47 A. Gaiduk, P. V. Ruijgrok, M. Yorulmaz and M. Orrit, *Phys. Chem. Chem. Phys.*, 2011, **13**, 149–153.
48 R. C. Maher, in *Raman Spectroscopy for Nanomaterials Characterization*, ed. C. S. S. R. Kumar, Springer, Berlin, Heidelberg, 2012.
49 S. L. Kleinman, R. R. Frontiera, A.-I. Henry, J. A. Dieringer and D. R. P. Van, *Phys. Chem. Chem. Phys.*, 2013, **15**, 21–36.
50 E. C. Le Ru, E. Blackie, M. Meyer and P. G. Etchegoin, *J. Phys. Chem. C*, 2007, **111**, 13794–13803.
51 J. P. Camden, J. A. Dieringer, Y. Wang, D. J. Masiello, L. D. Marks, G. C. Schatz and R. P. Van Duyne, *J. Am. Chem. Soc.*, 2008, **130**, 12616–12617.
52 S. M. Morton and L. Jensen, *J. Am. Chem. Soc.*, 2009, **131**, 4090–4098.
53 L. Jensen, C. M. Aikens and G. C. Schatz, *Chem. Soc. Rev.*, 2008, **37**, 1061–1073.
54 B. Sharma, R. R. Frontiera, A.-I. Henry, E. Ringe and R. P. Van Duyne, *Mater. Today*, 2012, **15**, 16–25.
55 S. Shim, C. M. Stuart and R. A. Mathies, *ChemPhysChem*, 2008, **9**, 697–699.
56 J. A. Dieringer, K. L. Wustholz, D. J. Masiello, J. P. Camden, S. L. Kleinman, G. C. Schatz and R. P. Van Duyne, *J. Am. Chem. Soc.*, 2008, **131**, 849–854.
57 M. Moskovits, *Phys. Chem. Chem. Phys.*, 2013, DOI: 10.1039/C2CP44030J.
58 J. Zhao, J. A. Dieringer, X. Zhang, G. C. Schatz and R. P. Van Duyne, *J. Phys. Chem. C*, 2008, **112**, 19302–19310.
59 S. Nie and S. R. Emory, *Science*, 1997, **275**, 1102–1106.
60 K. Kneipp, Y. Wang, H. Kneipp, L. T. Perelman, I. Itzkan, R. R. Dasari and M. S. Feld, *Phys. Rev. Lett.*, 1997, **78**, 1667–1670.
61 Y. R. Shen, *Nature*, 1989, **337**, 519–525.
62 P. Campagnola, *Anal. Chem.*, 2011, **83**, 3224–3231.
63 R. Jin, J. E. Jureller and N. F. Scherera, *Appl. Phys. Lett.*, 2006, **88**, 263111.
64 J. Butet, J. Duboisset, G. Bachelier, I. Russier-Antoine, E. Benichou, C. Jonin and P.-F. Brevet, *Nano Lett.*, 2010, **10**, 1717–1721.
65 G. Wang and N. Fang, *Methods Enzymol.*, 2012, **504**, 83–108.
66 G. Rong, H. Wang, L. R. Skewis and B. R. M. Reinhard, *Nano Lett.*, 2008, **8**, 3386–3393.
67 S. W. Hell, Single molecule spectroscopy in chemistry, physics and biology, in *Far-field optical nanoscopy*, ed. A. Gräslund, R. Rigler and J. Widengren, Springer, Berlin, Heidelberg, 2010, vol. 96.
68 T. Fujiwara, K. Ritchie, H. Murakoshi, K. Jacobson and A. Kusumi, *J. Cell Biol.*, 2002, **157**, 1071–1082.
69 L. B. Sagle, L. K. Ruvuna, J. M. Bingham, C. Liu, P. S. Cremer and R. P. Van Duyne, *J. Am. Chem. Soc.*, 2012, **134**, 15832–15839.
70 T. Hornung, J. Martin, D. Spetzler, R. Ishmukhametov and W. D. Frasch, *Methods Mol. Biol.*, 2011, **778**, 273–289.
71 G. Louit, T. Asahi, G. Tanaka, T. Uwada and H. Masuhara, *J. Phys. Chem. C*, 2009, **113**, 11766–11772.
72 R. L. Stiles, K. A. Willets, L. J. Sherry, J. M. Roden and R. P. Van Duyne, *J. Phys. Chem. C*, 2008, **112**, 11696–11701.
73 E. Ringe, J. M. McMahon, K. Sohn, C. M. Cobley, Y. Xia, J. Huang, G. C. Schatz, L. D. Marks and R. P. Van Duyne, *J. Phys. Chem. C*, 2010, **114**, 12511–12516.
74 J. M. McMahon, Y. Wang, L. J. Sherry, R. P. Van Duyne, L. D. Marks, S. K. Gray and G. C. Schatz, *J. Phys. Chem. C*, 2009, **113**, 2731–2735.
75 L. J. Sherry, S.-H. Chang, G. C. Schatz, R. P. Van Duyne, B. J. Wiley and Y. Xia, *Nano Lett.*, 2005, **5**, 2034–2038.
76 S. Zhang, K. Bao, N. J. Halas, H. Xu and P. Nordlander, *Nano Lett.*, 2011, **11**, 1657–1663.
77 C. Sönnichsen, T. Franzl, T. Wilk, G. von Plessen, J. Feldmann, O. Wilson and P. Mulvaney, *Phys. Rev. Lett.*, 2002, **7**, 077402.
78 H. Tamaru, H. Kuwata, H. T. Miyazaki and K. Miyano, *Appl. Phys. Lett.*, 2002, **80**, 1826–1828.
79 E. Ringe, M. R. Langille, K. Sohn, J. Zhang, J. Huang, C. A. Mirkin, R. P. Van Duyne and L. D. Marks, *J. Phys. Chem. Lett.*, 2012, **3**, 1479–1483.
80 A. Grubisic, E. Ringe, C. Cobley, Y. Xia, L. D. Marks, R. P. Van Duyne and D. J. Nesbitt, *Nano Lett.*, 2012, **12**, 4823–4829.
81 Y. Wang, S. K. Eswaramoorthy, L. J. Sherry, J. A. Dieringer, J. P. Cadmen, G. C. Schatz, R. P. Van Duyne and L. D. Marks, *Ultramicroscopy*, 2009, **109**, 1110–1113.
82 S. J. Barrow, A. M. Funston, D. E. Gómez, T. J. Davis and P. Mulvaney, *Nano Lett.*, 2011, **11**, 4180–4187.
83 A.-I. Henry, J. M. Bingham, E. Ringe, L. D. Marks, G. C. Schatz and R. P. Van Duyne, *J. Phys. Chem. C*, 2011, **115**, 9291–9305.
84 J. Zuloaga and P. Nordlander, *Nano Lett.*, 2011, **11**, 1280–1283.
85 A. L. Koh, A. I. Fernández-Domínguez, D. W. McComb, S. A. Maier and J. K. W. Yang, *Nano Lett.*, 2011, **11**, 1323–1330.
86 M.-W. Chu, V. Myroshnychenko, C. H. Chen, J.-P. Deng, C.-Y. Mou and F. J. G. D. Abajo, *Nano Lett.*, 2009, **9**, 399–404.
87 H. Okamoto and K. Imura, *Prog. Surf. Sci.*, 2009, **84**, 199–229.
88 M. De Serio, R. Zenobi and V. Deckert, *Trends Anal. Chem.*, 2003, **22**, 70–77.
89 A. Lewis, M. Isaacson, A. Harootunian and A. Muray, *Ultramicroscopy*, 1984, **13**, 227–231.
90 U. C. Fischer and D. W. Pohl, *Phys. Rev. Lett.*, 1989, **62**, 458–462.
91 K. Imura, H. Okamoto, M. K. Hossain and M. Kitajima, *Nano Lett.*, 2006, **6**, 2173–2176.
92 G. P. Wiederrecht, *Eur. Phys. J.: Appl. Phys.*, 2004, **28**, 3–18.
93 E. Betzig, J. K. Trautman, T. D. Harris, J. S. Weiner and R. L. Kostelak, *Science*, 1991, **251**, 1468–1470.

94 E. H. Synge, *Philos. Mag.*, 1928, **6**, 356–362.
95 R. M. Bakker, A. Boltasseva, Z. Liu, R. H. Pedersen, S. Gresillon, A. V. Kildishev, V. P. Drachev and V. M. Shalaev, *Opt. Express*, 2007, **21**, 13682–13688.
96 M. Rang, A. C. Jones, F. Zhou, Z.-Y. Li, B. J. Wiley, Y. Xia and M. B. Raschke, *Nano Lett.*, 2008, **8**, 3357–3363.
97 H. J. Lezec, A. Degiron, E. Devaux, R. A. Linke, L. Martin-Moreno, F. J. Garcia-Vidal and T. W. Ebbesen, *Science*, 2002, **297**, 820–822.
98 F. I. Baida and A. Belkhir, *Plasmonics*, 2009, **4**, 51–59.
99 S. Berweger, J. M. Atkin, R. L. Olmon and M. B. Raschke, *J. Phys. Chem. Lett.*, 2010, **1**, 3427–3432.
100 D. ten Bloemendal, P. Ghenuche, R. Quidant, I. G. Cormack, P. Loza-Alvarez and G. Badenes, *Plasmonics*, 2006, **1**, 41–44.
101 P. Ghenuche, S. Cherukulappurath and R. Quidant, *New J. Phys.*, 2008, **10**, 105013.
102 J. H. D. Eland, *Photoelectron Spectroscopy: An Introduction to Ultraviolet Photoelectron Spectroscopy in the Gas Phase*, Butterworths, London, 2nd edn, 1984.
103 L. Douillard, F. Charra, C. Fiorini, P. M. Adam, R. Bachelot, S. Kostcheev, G. Lerondel, M. Lamy de la Chapelle and P. Royer, *J. Appl. Phys.*, 2007, **101**, 083518.
104 A. Kubo, K. Onda, H. Petek, Z. Sun, Y. S. Jung and H. K. Kim, *Nano Lett.*, 2005, **5**, 1123–1127.
105 G. H. Fecher, O. Schmidt, Y. Hwu and G. Schönhense, *J. Electron Spectrosc. Relat. Phenom.*, 2002, **126**, 77–87.
106 L. Zhang, A. Kubo, L. Wang, H. Petek and T. Seideman, *Phys. Rev. B: Condens. Matter Mater. Phys.*, 2011, **84**, 245442.
107 M. Cinchetti, A. Gloskovskii, S. A. Nepjiko, G. Schönhense, H. Rochholz and M. Kreiter, *Phys. Rev. Lett.*, 2005, **95**, 047601.
108 S. J. Peppernick, A. G. Joly, K. M. Beck and W. P. Hess, *J. Chem. Phys.*, 2011, **134**, 034507.
109 T. Munakata, T. Masuda, N. Ueno, S. Sakaya, T. Sugiyama, N. Takehiro and Y. Sonoda, *Surf. Sci.*, 2003, **532–535**, 1140–1144.
110 M. Rohmer, M. Bauer, T. Leissner, C. Schneider, A. Fischer, G. Niedner-Schatteburg, B. von Issendorff and M. Aeschlimann, *Phys. Status Solidi B*, 2010, **247**, 1132–1138.
111 M. Aeschlimann, M. Bauer, D. Bayer, T. Brixner, S. Cunovic, F. Dimler, A. Fischer, W. Pfeiffer, M. Rohmer, C. Schneider, F. Steeb, C. Strüber and D. V. Voronine, *Proc. Natl. Acad. Sci. U. S. A.*, 2010, **107**, 5329–5333.
112 W. Wan, J. Feng, H. A. Padmore and D. S. Robin, *Nucl. Instrum. Methods Phys. Res., Sect. A*, 2004, **519**, 222–229.
113 V. Schweikhard, A. Grubisic, T. A. Baker, I. Thomann and D. J. Nesbitt, *ACS Nano*, 2011, **5**, 3724–3735.
114 V. Schweikhard, A. Grubisic, T. A. Baker and D. J. Nesbitt, *J. Phys. Chem. C*, 2011, **115**, 83–91.
115 O. L. A. Monti, T. A. Baker and D. J. Nesbitt, *J. Chem. Phys.*, 2006, **125**, 154709.
116 T. Coenen, E. J. R. Vesseur, A. Polman and A. F. Koenderink, *Nano Lett.*, 2011, **11**, 3779–3784.
117 L. Douillard and F. Charra, *J. Phys. D: Appl. Phys.*, 2011, **44**, 464002.
118 H. Duan, A. I. Fernández-Domínguez, M. Bosman, S. A. Maier and J. K. W. Yang, *Nano Lett.*, 2012, **12**, 1683–1689.
119 J. Nelayah, M. Kociak, O. Stéphan, F. J. García de Abajo, M. Tencé, L. Henrard, D. Taverna, I. Pastoriza-Santos, L. M. Liz-Marzán and C. Colliex, *Nat. Phys.*, 2007, **3**, 348–353.
120 O. Nicoletti, M. Wubs, N. A. Mortensen, W. Sigle, P. A. van Aken and P. A. Midgley, *Opt. Express*, 2011, **19**, 15371–15379.
121 S. Mazzucco, N. Geuquet, J. Ye, O. Stéphan, W. Van Roy, P. Van Dorpe, L. Henrard and M. Kociak, *Nano Lett.*, 2012, **12**, 1288–1294.
122 B. S. Guiton, V. Iberi, S. Li, D. N. Leonard, C. M. Parish, P. G. Kotula, M. Varela, G. C. Schatz, S. J. Pennycook and J. P. Camden, *Nano Lett.*, 2011, **11**, 3482–3488.
123 W. Van den Broek, J. Verbeeck, S. De Backer, P. Scheunders and D. Schryvers, *Ultramicroscopy*, 2006, **106**, 269–276.
124 K. Jarausch, P. Thomas, D. N. Leonard, R. Twesten and C. R. Booth, *Ultramicroscopy*, 2009, **109**, 326–337.
125 S. W. Prescott and P. Mulvaney, *J. Appl. Phys.*, 2006, **99**, 123504.
126 C. J. Murphy, T. K. Sau, A. M. Gole, C. J. Orendorff, J. Gao, L. Gou, S. E. Hunyadi and T. Li, *J. Phys. Chem. B*, 2005, **109**, 13857–13870.
127 K.-S. Lee and M. A. El-Sayed, *J. Phys. Chem. B*, 2006, **110**, 19220–19225.
128 Y. Xia, Y. Xiong, B. Lim and S. E. Skrabalak, *Angew. Chem., Int. Ed.*, 2009, **48**, 60–103.
129 C. M. Cobley, S. E. Skrabalak, D. J. Campbell and Y. Xia, *Plasmonics*, 2009, **4**, 171–179.
130 S. E. Skrabalak, L. Au, X. Li and Y. Xia, *Nat. Protocols*, 2007, **2**, 2182.
131 R. P. Van Duyne and J. P. Haushalter, *J. Phys. Chem.*, 1984, **88**, 2446–2451.
132 D. L. Jeanmaire and R. P. Van Duyne, *J. Electroanal. Chem.*, 1977, **84**, 1–20.
133 A. D. McFarland, M. A. Young, J. A. Dieringer and R. P. Van Duyne, *J. Phys. Chem. B*, 2005, **109**, 11279–11285.
134 M. Kahl, E. Voges, S. Kostrewa, C. Viets and W. Hill, *Sens. Actuators, B*, 1998, **51**, 285–291.
135 J. R. Lakowicz, C. D. Geddes, I. Gryczynski, J. Malicka, Z. Gryczynski, K. Alsan, J. Lukomska, E. Matveeva, J. Zhang, R. Badugu and J. Huang, *J. Fluoresc.*, 2004, **14**, 425–441.
136 A. J. Haes, S. Zou, J. Zhao, G. C. Schatz and R. P. Van Duyne, *J. Am. Chem. Soc.*, 2006, **128**, 10905–10914.
137 J. Zhao, A. Das, X. Zhang, G. C. Schatz, S. G. Sligar and R. P. Van Duyne, *J. Am. Chem. Soc.*, 2006, **128**, 11004–11005.
138 J. J. Mock, M. Barbic, D. R. Smith, D. A. Schultz and S. Schultz, *J. Chem. Phys.*, 2002, **116**, 6755–6759.
139 I. Pastoriza-Santos and L. M. Liz-Marzán, *J. Mater. Chem.*, 2008, **18**, 1724–1737.
140 K. Munechika, J. M. Smith, Y. Chen and D. S. Ginger, *J. Phys. Chem. C*, 2007, **111**, 18906–18911.
141 M. Hu, J. Chen, M. Marquez, Y. Xia and G. V. Hartland, *J. Phys. Chem. C*, 2007, **111**, 12558–12565.
142 T. Itoh, T. Uwada, T. Asahi, Y. Ozaki and H. Masuhara, *Can. J. Anal. Sci. Spectrosc.*, 2007, **52**, 130–141.

143 C. L. Nehl, N. K. Grady, G. P. Goodrich, F. Tam, N. J. Halas and J. H. Hafner, *Nano Lett.*, 2004, **4**, 2355–2359.
144 F. Zhou, Z.-Y. Li, Y. Liu and Y. Xia, *J. Phys. Chem. C*, 2008, **112**, 20233–20240.
145 B. J. Wiley, Y. Chen, J. M. McLellan, Y. Xiong, Z.-H. Li, D. Ginger and Y. Xia, *Nano Lett.*, 2007, **7**, 1032–1036.
146 H. Wang, D. W. Brandl, F. Le, P. Nordlander and N. J. Halas, *Nano Lett.*, 2006, **6**, 827–832.
147 H. Wei, A. Reyes-Coronado, P. Nordlander, J. Aizpurua and H. Xu, *ACS Nano*, 2010, **4**, 2649–2654.
148 J. M. J. Santillán, L. B. Scaffardi and D. C. Schinca, *J. Phys. D: Appl. Phys.*, 2011, **44**, 105104.
149 E. Ringe, J. Zhang, M. R. Langille, C. A. Mirkin, L. D. Marks and R. P. V. Duyne, *Nanotechnology*, 2012, **23**, 444005.
150 L. M. Liz-Marzán, *Langmuir*, 2006, **22**, 32–41.
151 J. J. Mock, D. R. Smith and S. Schultz, *Nano Lett.*, 2003, **3**, 485–491.
152 L. J. Sherry, R. Jin, C. A. Mirkin, G. C. Schatz and R. P. Van Duyne, *Nano Lett.*, 2006, **6**, 2060–2065.
153 P. H. C. Camargo, M. Rycenga, L. Au and Y. Xia, *Angew. Chem., Int. Ed.*, 2009, **48**, 2180–2184.
154 E. D. Dielbold, P. Peng and E. Mazur, *J. Am. Chem. Soc.*, 2009, **131**, 16356–16357.
155 M. Rycenga, X. Xia, C. H. Moran, F. Zhou, D. Qin, Z.-Y. Li and Y. Xia, *Angew. Chem., Int. Ed.*, 2011, **50**, 5473–5477.
156 K. L. Wustholz, A.-I. Henry, J. M. McMahon, R. G. Freeman, N. Valley, M. E. Piotti, M. J. Natan, G. C. Schatz and R. P. Van Duyne, *J. Am. Chem. Soc.*, 2010, **132**, 10903–10910.
157 F. J. García de Abajo and M. Kociak, *Phys. Rev. Lett.*, 2008, **100**, 106804.
158 U. Hohenester, H. Ditlbacher and J. R. Krenn, *Phys. Rev. Lett.*, 2009, **103**, 106801.
159 A.25 Bouhelier, G. Colas des Francs and J. Grandidier, in *Plasmonics, Springer Series in Optical Sciences 167*, ed. S. Enoch and N. Bonod, Springer-Verlag, Berlin, Heidelberg, 2012.
160 E. J. R. Vesseur, R. de Waele, M. Kuttge and A. Polman, *Nano Lett.*, 2007, **7**, 2843–2846.
161 A. Bouhelier, R. Bachelot, G. Lerondel, S. Kostcheev, P. Royer and G. P. Wiederrecht, *Phys. Rev. Lett.*, 2005, **95**, 267405.
162 L. Tong, T. Zhu and Z. Liu, *Chem. Soc. Rev.*, 2011, **40**, 1296–1304.
163 C. E. Talley, J. B. Jackson, C. Oubre, N. K. Grady, C. W. Hollars, S. M. Lane, T. R. Huser, P. Nordlander and N. J. Halas, *Nano Lett.*, 2005, **5**, 1569–1574.
164 L.-L. Tay, J. Hulse, D. Kennedy and J. P. Pezacki, *J. Phys. Chem. C*, 2010, **114**, 7356–7363.
165 L. Rodríguez-Lorenzo, R. N. A. Álvarez-Puebla, I. Pastoriza-Santos, S. Mazzucco, O. Stéphan, M. Kociak, L. M. Liz-Marzán and F. J. García de Abajo, *J. Am. Chem. Soc.*, 2009, **131**, 4616–4618.
166 P. Aldeanueva-Potel, E. Carbó-Argibay, N. Pazos-Pérez, S. Barbosa, I. Pastoriza-Santos, R. A. Alvarez-Puebla and L. M. Liz-Marzán, *ChemPhysChem*, 2012, **13**, 2561–2565.
167 J. M. McLellan, Z.-Y. Li, A. R. Siekkinen and Y. Xia, *Nano Lett.*, 2007, **7**, 1013–1017.
168 M. J. Mulvihill, X. Y. Ling, J. Henzie and P. Yang, *J. Am. Chem. Soc.*, 2010, **132**, 268–274.
169 M. Rycenga, P. H. C. Camargo, W. Li, C. H. Moran and Y. Xia, *J. Phys. Chem. Lett.*, 2010, **1**, 696–703.
170 G. H. Chan, J. Zhao, E. M. Hicks, G. C. Schatz and R. P. Van Duyne, *Nano Lett.*, 2007, **7**, 1947–1952.
171 L.-X. Qin, C. Jing, Y. Li, D.-W. Li and Y.-T. Long, *Chem. Commun.*, 2012, **48**, 1511–1513.
172 J. Cheng, Y. Liu, X. Cheng, Y. He and E. S. Yeung, *Anal. Chem.*, 2010, **82**, 8744–8749.
173 C. Novo, A. M. Funston, A. K. Gooding and P. Mulvaney, *J. Am. Chem. Soc.*, 2009, **131**, 14664–14666.
174 C. Novo, A. M. Funston and P. Mulvaney, *Nat. Nanotechnol.*, 2008, **3**, 598–602.
175 D. Seo, G. Park and H. Song, *J. Am. Chem. Soc.*, 2011, **134**, 1221–1227.
176 N. Liu, M. L. Tang, M. Hentschel, H. Giessen and A. P. Alivisatos, *Nat. Mater.*, 2011, **10**, 631–636.
177 Y. Li, C. Jing, L. Zhang and Y.-T. Long, *Chem. Soc. Rev.*, 2012, **41**, 632–642.
178 X. Nan, P. A. Sims and X. S. Xie, *ChemPhysChem*, 2008, **9**, 707–712.
179 L. Xiao, Y. Qiao, Y. He and E. S. Yeung, *Anal. Chem.*, 2010, **82**, 5268–5274.
180 C. J. DeSantis and S. E. Skrabalak, *Langmuir*, 2012, **28**, 9055–9062.
181 C. J. DeSantis, A. C. Sue, M. M. Bower and S. E. Skrabalak, *ACS Nano*, 2012, **6**, 2617–2628.
182 N. Liu, M. Hentschel, T. Weiss, A. P. Alivisatos and H. Giessen, *Science*, 2011, **332**, 1407–1410.
183 M. A. Schmidt, D. Y. Lei, L. Wondraczek, V. Nazabal and S. A. Maier, *Nat. Commun.*, 2012, **3**, 1108.
184 E. C. Le Ru and P. G. Etchegoin, *Annu. Rev. Phys. Chem.*, 2012, **63**, 65–87.
185 S. K. Kleinman, E. Ringe, N. Valley, K. L. Wustholz, E. Phillios, K. A. Scheidt, G. C. Schatz and R. P. Van Duyne, *J. Am. Chem. Soc.*, 2011, **133**, 4115–4122.
186 J. A. Dieringer, R. B. Lettan, K. A. Scheidt and R. P. Van Duyne, *J. Am. Chem. Soc.*, 2007, **129**, 16249–16256.
187 A. Otto, *J. Raman Spectrosc.*, 2002, **33**, 593–598.
188 A. J. Haes and R. P. Van Duyne, *Anal. Bioanal. Chem.*, 2004, **379**, 920–930.
189 N. G. Khlebtsov and L. A. Dykman, *J. Quant. Spectrosc. Radiat. Transfer*, 2010, **111**, 1–35.
190 K. Kneipp, H. Kneipp and J. Kneipp, *Acc. Chem. Res.*, 2006, **39**, 443–450.